Forensic Chemistry 19 (2020) 100245

Contents lists available at ScienceDirect

Forensic Chemistry

journal homepage: www.elsevier.com/locate/forc

Identification of novel fragmentation pathways and fragment ion structures in the tandem mass spectra of protonated synthetic cathinones

J. Tyler Davidson[a], Elettra L. Piacentino[b], Zachary J. Sasiene[c], Younis Abiedalla[d], Jack DeRuiter[d], C. Randall Clark[d], Giel Berden[e], Jos Oomens[e], Victor Ryzhov[b], Glen P. Jackson[a,c,*]

[a] Department of Forensic and Investigative Science, West Virginia University, Morgantown, WV 26506-6121, USA
[b] Department of Chemistry and Biochemistry, Northern Illinois University, DeKalb, IL, 60115, USA
[c] C. Eugene Bennett Department of Chemistry, West Virginia University, Morgantown, WV 26506-6121, USA
[d] Department of Drug Discovery and Development, Harrison School of Pharmacy, Auburn University, Auburn, AL 36849, USA
[e] Radboud University, Institute for Molecules and Materials, FELIX Laboratory, Toernooiveld 7, 6525 ED Nijmegen, the Netherlands

HIGHLIGHTS

- Pathway(s) rationalized for the base peak in the tandem mass spectra of many synthetic cathinones.
- High mass accuracy established elemental composition of fragments.
- Isotope labeling and MS^n established consecutive fragmentation pathways.
- Ion spectroscopy and theoretical calculations supported the identity of proposed phthalate-like intermediates.

ARTICLE INFO

Keywords:
Tandem mass spectrometry
Isotope labeling
Ion spectroscopy
DFT calculations
Cathinones

ABSTRACT

The expanding use of emerging synthetic drugs such as synthetic cathinones, or "bath salts", is a growing public health concern and a continual challenge for drug analysts. In the tandem mass spectra of protonated α-pyrrolidinophenone cathinones, the tropylium ion at *m/z* 91 is often among the most abundant product ions, but its mechanistic origin is currently unexplained. This project combined electrospray ionization multi-stage mass spectrometry (ESI-MS^n), high-resolution mass spectrometry (HRMS), isotopic labeling and ion spectroscopy to enhance our understanding of the fragmentation pathways and mechanisms of a variety of α-pyrrolidinophenone cathinones. The fragmentation trends derived from these ESI-MS/MS studies are: 1) unlike *N*-alkylated cathinones, abundant radical cations are not observed from even-electron precursors of α-pyrrolidinophenones; 2) the loss of a 71 Da pyrrolidine neutral to form an alkylphenone cation is always observed; 3) a series of neutral alkenes are lost from the alkylphenone cation to form intermediate cations with phthalane-like structures. The phthalane intermediates then eliminate the carbonyl carbon as CO or C_2H_2O to form a tropylium ion at *m/z* 91. The α-carbon of the original cathinone is almost exclusively retained in the tropylium ion. If the original cathinone is substituted on the aromatic ring, the observed tropylium ion will be shifted by the mass of the substitution. These findings explain the characteristic ions in ESI-MS/MS spectra of synthetic cathinones and will help analysts better employ mass spectral observations in future casework.

1. Introduction

Synthetic cathinones are members of a larger class of novel psychoactive substances (NPS) commonly referred to as "designer drugs" or "legal highs" [1]. They are phenylalkylamine derivatives, closely related to amphetamines, which produce stimulant-like pharmacological effects. These effects drive the recreational use of synthetic cathinones, which are often marketed as "not for human consumption" or "bath salts" to avoid legislative restrictions [1–4]. Cathinones are analogs of the natural psychoactive chemical cathinone, which is present in the leaves of the *Catha edulis* plant, commonly known as khat. This plant is native to the Horn of Africa and the Southwest Arabian Peninsula. Traditionally, khat leaves have been chewed for their stimulant-like effects and used in religious ceremonies such as funerals

* Corresponding author. Tel.: 304 293 9236.
E-mail address: glen.jackson@mail.wvu.edu (G.P. Jackson).

https://doi.org/10.1016/j.forc.2020.100245
Received 15 January 2020; Received in revised form 25 March 2020; Accepted 6 April 2020
Available online 11 April 2020

and weddings [1]. As trade routes expanded, knowledge about the stimulant-like properties of khat leaves extended to Europe and the Western world [5,6].

The first synthetic cathinones to appear on the market in the early twentieth century were originally designed for therapeutic purposes, but recreational use has taken over in the last decade [6,7]. Synthetic cathinones are sold in the form of white or yellow amorphous or crystalline powder or in capsules. The quantities usually range from 50 mg to 500 mg packages and the price varies between $25-$50 per 50 mg [4,8,9]. Common brand names include Bloom, Blue Silk, Ivory Wave, Purple Wave, and Vanilla Sky [1,4].

Once synthetic cathinones started to flood the market, countries began to enact legislative restrictions. By 2011 several synthetic cathinones were provisionally scheduled under Schedule I of the United States Controlled Substances Act [7,10]. However, the regulation of synthetic cathinones is complicated by the sheer diversity of chemical modifications that are continuously adopted to avoid the regulations imposed on existing analogs [1]. Due to the lag in regulations behind the drugs currently available on the market it is imperative to recognize the characteristic fragmentation of synthetic cathinones and understand the fragmentation pathways through which mass spectra are generated.

Four common families of synthetic cathinones can be identified based on the location of substitution to the core synthetic cathinone structure. The first family of synthetic cathinones are analogs that are *N*-alkylated at the amine moiety, some of which contain ring substituents [1,11]. These substances were primarily derived for their therapeutic properties, such as antidepressants. A second family of synthetic cathinones is the pyrrolidinophenone-like family, which are characterized by a pyrrolidinyl substitution at the amine moiety [12]. Another family of synthetic cathinones involves methylation at the α-carbon adjacent to the amine nitrogen in the generic synthetic cathinone structure. The last family of synthetic cathinones has both the 3,4-methylenedioxy ring substitution and the *N*-pyrrolidinyl moiety [7]. One common variation for all families of synthetic cathinones is varying lengths of the alkyl chains branching from the α-carbon.

Whereas many laboratories and research articles conduct routine mass spectrometric analysis of synthetic cathinones, the underlying fragmentation mechanisms that lead to the observed fragment ions are rarely described or understood. However, analysts recognize that structural similarities of synthetic cathinones tend to provide mass-spectral similarities, which greatly assists in the interpretation of spectra of novel synthetic cathinones.

The seized drug community typically employs gas chromatography-electron ionization-mass spectrometry (GC-EI-MS) to identify unknowns whereas the toxicological community often employs liquid chromatography with electrospray ionization and tandem mass spectrometry (LC-ESI-MS/MS). Due to differences in the ionization mechanisms, electron ionization (EI) primarily produces odd-electron ions and ESI primarily produces even-electron ions. The differences in electron parity and energy deposition typically results in major differences in the fragment mass spectra, as has been demonstrated for a variety of synthetic cathinones [13–18]. For example, Sauer et al. [19] and Abiedalla et al. [20] report the absence of ions at *m/z* 91 and *m/z* 135 for α-PVP and 3,4-MDPV (see Table 1 for full names) under EI-MS conditions, but Hasegawa et al. [21] and Fornal [16] report the presence of both ions under ESI-MS/MS conditions.

The analysis of synthetic cathinones with ESI-MS/MS reveals the tropylium ion (*m/z* 91) or methylenedioxy analog (*m/z* 135) as one of the most abundant ions in the protonated tandem mass spectra of many synthetic cathinones [22–25]. Despite the importance of the tropylium ion or methylenedioxy-analog ion in the product ion spectra of synthetic cathinones, previous attempts to explain the mechanistic origin of these important diagnostic ions have been inadequate. As examples, in the first report on the fragmentation of protonated PV8, Swortwood et al. do not address the mechanism of formation of the tropylium ion [26]. In a previous work, Ibanez et al. propose an unsupported 'shift' of the carbonyl group to explain the equivalent ion at *m/z* 135 for 3,4-MDPV [27]. Similarly, Pozo et al., Fabregat-Safont et al., and Qian et al. propose mechanisms that involve the loss of CO directly from the aliphatic chain during the fragmentation of synthetic cathinones without the use of isotopic labeling to support these conclusions [28–30]. Our work now supports these proposed losses of CO.

In all the above cases, the mechanism(s) are either absent, ambiguous or unsupported with experimental data. A similar problem with the existing knowledge of synthetic cathinone fragmentation is exemplified by accurate mass studies involving methcathinone and ethcathinone fragmentation [31,32]. Bijlsma et al. showed an unexpected product ion at *m/z* 105.0740, which must have the elemental composition $C_8H_9^+$ [31]. The ion is unexpected because its occurrence requires multiple rearrangements. However, the article did not describe the use of isotope labeling or MS^n experiments, so the mechanism of formation of the $C_8H_9^+$ fragment remains unclear. The observation of both *m/z* 105.0334 and *m/z* 105.0697 from ethcathinone also indicates extensive covalent rearrangements that remain unexplained [32].

These articles demonstrate that there is a significant lack of understanding in the fragmentation behavior of synthetic cathinones with ESI-MS/MS. To better defend the observations of existing casework, to better understand the current observations, and to better predict the fragmentation patterns of future synthetic cathinones, this project examines the fragmentation behavior of synthetic cathinones generated via ESI and analyzed with both ion trap (IT) and quadrupole time-of-flight (Q-TOF) mass spectrometers. IT mass spectrometers are typically nominal mass instruments, but they have the capability to perform multiple stages of mass spectrometry. In contrast, Q-TOF mass spectrometers are high-resolution instruments that provide accurate mass measurements. The combination of multi-stage mass spectrometry (MS^n), accurate mass measurements with high-resolution mass spectrometry (HRMS), isotopic labeling and gas-phase infrared ion spectroscopy allows for the confirmation of intermediate product ions along the proposed fragmentation pathways and provides support for our proposed mechanisms. The identification of a novel fragmentation pathway(s) for the generation of the tropylium ion or methylenedioxy-analog ion provides a more coherent framework of understanding for the identification of future synthetic cathinone analogs.

2. Methods

2.1. Sample preparation

This study involved the analysis of 11 synthetic cathinones that were purchased through Cayman Chemical (Ann Arbor, MI, USA) and 11 isotopically labeled or non-commercially available synthetic cathinones synthesized in-house at Auburn University. Table 1 contains the synthetic cathinones analyzed in this study.

Before the synthetic samples were shipped to West Virginia University, a full characterization using NMR and GC-EI-MS was performed at Auburn University to confirm the correct labeling and assess the level of chemical and isotopic impurities in the purified products. In general, the GC total ion chromatograms (TIC) and NMR spectra indicated that the purity of the target compound was typically greater than 95%. Isotopic impurities do not interfere with the tandem mass spectrometry results because the isotopic impurities are excluded during isolation of a specific precursor isotope. Synthetic procedures, EI-MS spectra and NMR data are available on request.

All samples were analyzed at a concentration of approximately 100 ppm. The non-deuterated samples were dissolved in a solution of 49% HPLC grade methanol, 49% distilled water and 2% acetic acid. Deuterated samples were dissolved in HPLC grade methanol only to prevent back exchange. The HPLC-grade methanol was supplied by Fisher Scientific (Palo Alto, CA, USA) and the acetic acid was supplied by Acros Organics (Palo Alto, CA, USA).

Table 1
Synthetic cathinones analyzed in this study.

Cayman Chemical	Synthesized at Auburn University
α-pyrrolidinopropiophenone (α-PPP)	^{13}C-α-pyrrolidinovalerophenone labeled on the carbonyl carbon (^{13}C-carbonyl carbon-α-PVP)
α-pyrrolidinobutiophenone (α-PBP)	^{13}C-α-pyrrolidinovalerophenone labeled on the α-carbon (^{13}C-α-carbon-α-PVP)
α-pyrrolidinovalerophenone (α-PVP)	^{18}O-α-pyrrolidinovalerophenone (^{18}O-α-PVP)
α-pyrrolidinoheptanophenone (PV8)	α-pyrrolidinovalerophenone-d_7 labeled on the alkyl chain (α-PVP-d_7)
4-methoxy-α-pyrrolidinopentiophenone (4-MeO-α-PVP)	α-pyrrolidinovalerophenone-d_8 labeled on the pyrrolidine ring (α-PVP-d_8)
3′,4′-trimethylene-α-pyrrolidinovalerophenone	α-methyl-pyrrolidinovalerophenone (α-PVP-methyl group)
3,4-methylenedioxy-α-pyrrolidinopropiophenone (3,4-MDPPP)	^{13}C-α-pyrrolidinoheptanophenone labeled on the carbonyl carbon (^{13}C-PV8)
3,4-methylenedioxy-α-pyrrolidinobutiophenone (3,4-MDPBP)	^{13}C-α-pyrrolidinopropiophenone on the α-carbon (^{13}C-α-PPP)
3,4-methylenedioxypyrovalerone (3,4-MDPV)	^{13}C-4′-methyl-α-pyrrolidinohexanophenone on the carbonyl carbon (^{13}C-MPHP)
3,4-methylenedioxypyrovalerone-d_8 on the pyrrolidine ring (3,4-MDPV-d_8)	^{13}C-3,4-methylenedioxypyrovalerone on the carbonyl carbon (^{13}C-3,4-MDPV)
2,3-methylenedioxypyrovalerone (2,3-MDPV)	^{13}C-Naphyrone on the carbonyl carbon

2.2. Instrumentation

2.2.1. Velos Pro linear ion trap

A Thermo Scientific Velos Pro linear ion trap (LIT) mass spectrometer was operated with heated-electrospray ionization (HESI). The HESI source was operated at 50 °C with a spray voltage of 4,000 V. The nitrogen sheath gas was operated at 8 arbitrary units with a nitrogen auxiliary gas flow of 5 arbitrary units. The mass spectrometer capillary temperature was 275 °C. The scan range and normalized collision energy (NCE) were different for each compound and are labeled with each mass spectrum. Ultra-pure helium was used as the bath gas purchased through Matheson TRIGAS (Fairmont, WV, USA).

2.2.2. Agilent Technologies 6538 UHD accurate-mass quadrupole time-of-flight (Q-TOF)

An Agilent Technologies 6538 UHD Accurate-Mass Quadrupole Time-of-Flight (Q-TOF) mass spectrometer was operated with a dual ESI source at a spray voltage of 3,500 V. The nitrogen gas was set to 300 °C with a drying gas flow of 5 L/min and a nebulizer flow of 30 psig. The MS fragmentor and skimmer voltages were operated at 225 V and 65 V, respectively. The scan range and collision energy were different for each compound and are labeled in each mass spectrum. An isolation width of 1.3 Da was used for all samples. Ultra-pure nitrogen was used for the collision gas purchased through Matheson TRIGAS (Fairmont, WV, USA).

2.2.3. Ion spectroscopy

Gas-phase infrared ion spectroscopy experiments were performed at the FELIX laboratory in Nijmegen, Netherlands using an electrospray ionization source on a Bruker Amazon ion trap mass spectrometer, modified to provide optical access to the trapped ions [33]. The flow rate of the α-PVP sample to the source was 120 μL/h with a spray voltage of −4500 V and N_2 nebulizer gas was used. Precursor ions at *m/z* 119 and *m/z* 133 were generated through ESI-MS/MS of α-PVP (fragmentation of $[M+H]^+$ at *m/z* 232), isolated in the ion trap and irradiated with 10 infrared laser pulses from the free electron laser (FEL) (repetition rate 10 Hz, pulse energies between 80 and 200 mJ), which was tuned over the frequency range 1000–1850 cm^{-1}. The recorded mass spectra were used to determine the infrared multiple photon dissociation (IRMPD) yield at each wavelength, which is defined as the ratio of the summed product ion intensities divided by the total ion intensity. After measuring the intensities of the precursor and fragment ions at a given wavelength of irradiation, the IR frequency was changed in steps of 3 cm^{-1}. For each IR frequency, new packets of ions were loaded into the ion trap and irradiated. The intensities of the precursor and product ions were the average of five replicate mass spectra per IR step. The whole process continued across the fingerprint spectral region (1000–1850 cm^{-1}). IRMPD spectra were linearly corrected for variations in laser power as a function of IR frequency. The experimental gas-phase IRMPD spectra could then be compared to the density functional theory (DFT) calculated spectra.

The lowest-energy geometry was calculated at the B3LYP/6-311 + G(d,p) level of theory using Gaussian 09 [34] for several isomeric structures of each of the two intermediate product ions at *m/z* 119 (Supplemental Fig. 1) and *m/z* 133 (Supplemental Fig. 2). The Cartesian coordinates for the optimized isomeric structures for the product ions at *m/z* 119 and *m/z* 133 are presented in Supplemental Table 1 and Supplemental Table 2, respectively. The vibrational frequencies calculated at this level of theory provided thermodynamic corrections to the raw energies and the theoretical vibrational spectra of each species. Comparison of the calculated and the IRMPD spectra, along with the relative energies between isomers, provided justification for the assignment of the most probable isomer of each species.

2.3. Data analysis

Xcalibur 2.0.0.48 software was used for the data analysis on the Velos Pro and Mass Hunter Qualitative Analysis B.05.00 was used for the Agilent Q-TOF data analysis. Microsoft Excel version 14 (Microsoft, Redmond, WA, USA) and ChemDraw 16.0 (PerkinElmer, Waltham, MA, USA) were used for mass spectral plots and mass spectral fragmentation mechanisms, respectively.

2.3.1. Mass spectral interpretation and mechanisms

The proposed fragmentation mechanisms in the following section are based on MS^n analyses, rational electron pushing mechanisms and the expected lowest energy pathways [35]. Whereas the identification of the exact hydrogen(s) in a specific rearrangement is not always possible in this study, deuterium labeling was often able to exclude the involvement of certain hydrogen atoms. The use of MS^n permits the structural determination of all the intermediates along a fragmentation pathway, so even when the exact structure of an intermediate is not known, it is still possible to generate a deeper understanding of the precursors and products of a certain intermediate than the present status. Odd-electron product ions formed from even-electron (i.e. protonated) precursor ions of synthetic cathinones have been reported before by Fornal [36,37], but none of the α-pyrrolidinophenone synthetic cathinones analyzed in this study provided a significant abundance of odd-electron product ions, which is consistent with previous literature [36].

3. Results and discussion

Since the seminal publication by Rylander et al. in 1956 [38], the propensity of aromatic compounds to form energetically favored tropylium fragments has been studied extensively in EI-MS spectra. The original article recognized the thermodynamic and tautomeric benefits of rearrangement of the benzylium ion ($C_7H_7^+$, *m/z* 91) to the tropylium ion, which is a constitutional isomer. In the 1970s, McLafferty et al. focused on the formation of tropylium ions from a variety of alkyl-substituted benzenes under EI-MS conditions [39,40] McLafferty and coworkers showed that whereas benzylium and tropylium ions are

often equally favored at threshold fragmentation energies, the tropylium ion is favored by a factor of at least 2:1 at EI energies around 70 eV [39,40].

Lifshitz et al. also demonstrated that the tropylium ion is more stable than several other isomers and noticeably lower in energy than the benzylium ion, which explains the preference for the ring expansion of benzylium ions to the tropylium ion structure [41]. More recently, Hayward et al. have described the formation of the tropylium ion with surface-induced dissociation (SID) [42]. Hayward et al. showed that the ring expansion from the benzylium ion to the tropylium ion was exothermic and often involves the incorporation of alkyl substituents. Specifically, the reaction of neutralized benzene with sputtered $C_3H_5^+$ followed by the loss of ethene was the most likely route for tropylium ion formation [42]. Using a variety of theoretical calculations, several groups have shown that the activation barrier from the benzylium ion to the tropylium ion is in the range of 1.4–3.4 eV and that the tropylium ion is thermodynamically more stable than the benzylium ion by approximately 0.37 eV [43–49]. Although the mechanism(s) from the benzylium ion to tropylium ion is therefore very well documented, mechanisms to form the tropylium ion from aromatic ketones—like alkylphenones and cathinones—have not been adequately described. We therefore conducted various experiments to rationalize the significant rearrangements that are required to produce the tropylium ion from a variety of synthetic cathinones.

3.1. HESI-Velos Pro MS^n

Fig. 1 shows the MS^n fragmentation of α-PVP with the major structural fragments embedded. Isolation and fragmentation of the precursor ion $[M+H]^+$ at *m/z* 232 results in the primary product ions at *m/z* 214, 189, 161, and 154 (Fig. 1a). The base peak of this spectrum is observed at *m/z* 161, which is formed through the loss of the pyrrolidine ring from the precursor ion. Fig. 1b shows the product ions produced from the isolation and fragmentation of the primary product ion at *m/z* 161. The main product ions are observed at *m/z* 143, 133, 119, 105, and 91.

Based on the MS^n analysis of *m/z* 161, the secondary product ions at *m/z* 143, 133, and 119 are formed through the loss of H_2O, ethylene or CO, and propylene, respectively. Fig. 1c shows the isolation and fragmentation of the secondary product ion at *m/z* 119, which results in the exclusive formation of the tropylium ion at *m/z* 91, which can only occur through the loss of CO from the intermediate at *m/z* 119.

Fig. 2 shows the MS^n fragmentation of α-PVP that has a ^{13}C label on the carbonyl carbon. The structures of major fragments are also embedded in Fig. 2. Evidence for the phthalane structure shown in Fig. 2b is provided by ion spectroscopy and DFT calculations in section 3.4. Isolation and fragmentation of the isotope-labeled precursor ion $[M+H]^+$ at *m/z* 233 (Fig. 2a) results in a variety of ions, including *m/z* 162, 133, 120, 106, and 91. Following the same logic as Fig. 1, the structure at *m/z* 162 corresponds to the loss of the pyrrolidine ring from the precursor. The product ions formed through the isolation and fragmentation of *m/z* 162 (Fig. 2b) include *m/z* 144, 134, 133, 120, 106, 105, and 91. Based on MS^n analyses, the ^{13}C-labeled carbonyl carbon is not incorporated into the tropylium ion and must be lost as neutral ^{13}CO (Fig. 2c).

The observation of the intermediate at *m/z* 133 in the MS^2 and MS^3 spectra of Fig. 2a and 2b, respectively, is particularly interesting. Although the loss of CO directly from the alkyl chain had been proposed

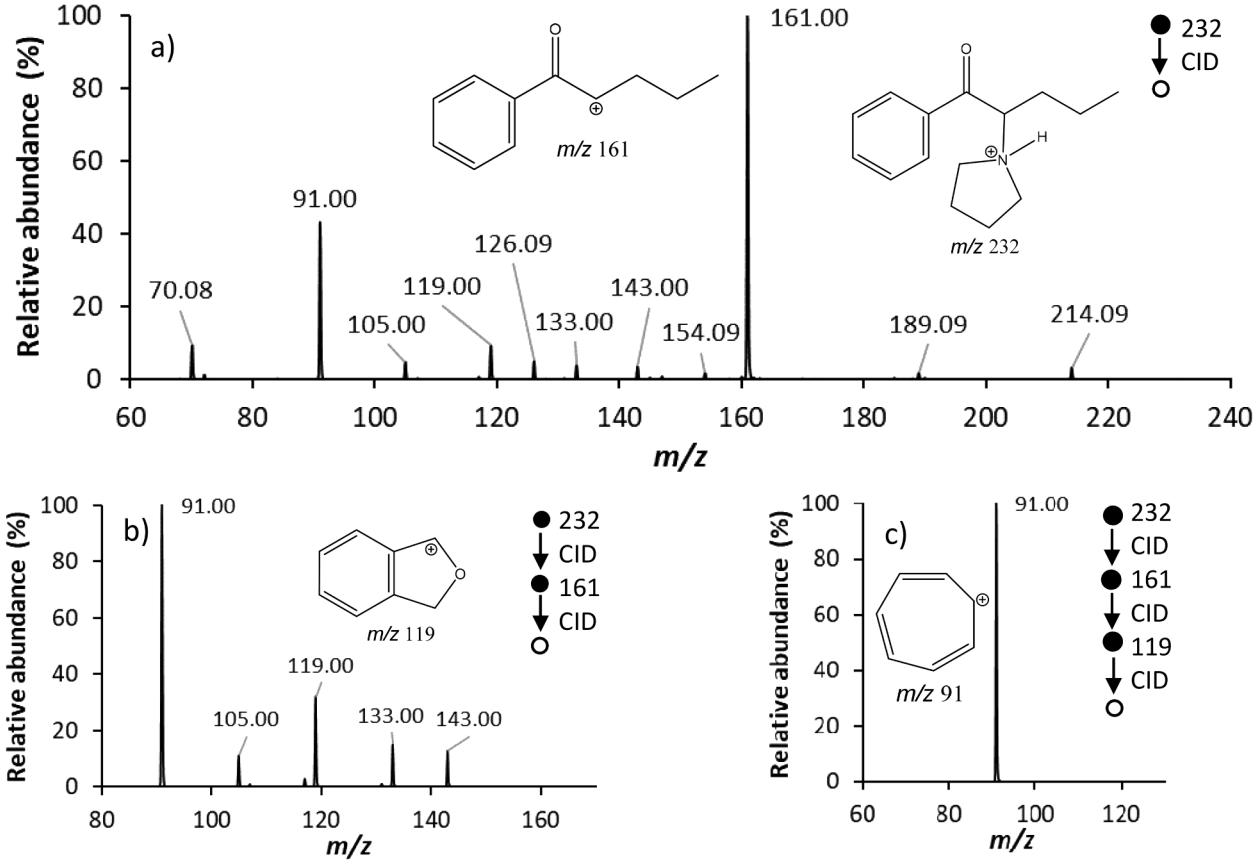

Fig. 1. Tandem mass spectra of α-PVP: a) MS^2 product ion spectrum of the $[M+H]^+$ molecular ion (35% NCE); b) MS^3 product ion spectrum of the product ion at *m/z* 161 (30% NCE) showing the formation of product ions at *m/z* 143, 133, 119, 105, and 91; c) MS^4 product ion spectrum of the secondary product ion at *m/z* 119 (30% NCE) showing the formation of only the tropylium ion at *m/z* 91. Evidence for the phthalane structure shown in panel b) is provided by ion spectroscopy and DFT calculations in section 3.4.

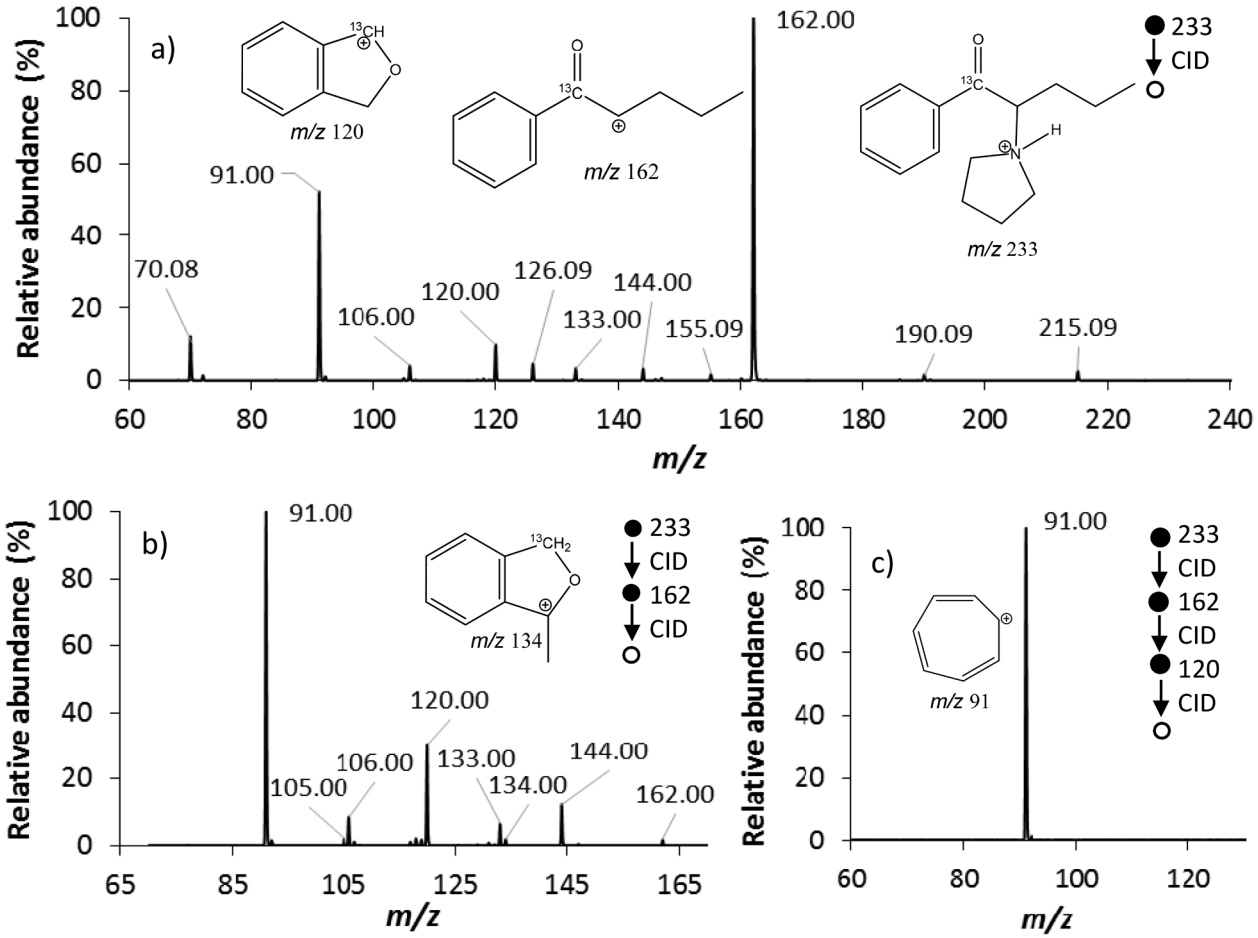

Fig. 2. Tandem mass spectra of ^{13}C-carbonyl labeled α-PVP: a) MS^2 product ion spectrum of the $[M+H]^+$ molecular ion (35% NCE); b) MS^3 spectrum of the intermediate ion at *m/z* 162 (30% NCE); c) MS^4 spectrum of the intermediate ion at *m/z* 120 (30% NCE) showing the formation of only the secondary product ion at *m/z* 91. Evidence for the phthalane structures in panels a) and b) are provided by ion spectroscopy and DFT calculations in section 3.4.

by Pozo et al. [28], Fabregat-Safont et al. [29] and Qian et al. [30], this pathway had not been verified until the current use of isotopic labeling.

The MS^n fragmentation of the precursor ion $[M+H]^+$ at *m/z* 234 for ^{18}O-α-PVP results in the formation of primary product ions at *m/z* 214, 191, 163, and 156 (Fig. 3a). The primary product ions, except for *m/z* 214, are all shifted by two Daltons (Da) relative to the same product ions for α-PVP, which appear at *m/z* 189, 161, and 154. This observed 2 Da shift indicates these fragments must include the ^{18}O-labeled oxygen. In contrast, the primary product ion at *m/z* 214 must not contain the ^{18}O label. The product at *m/z* 214 can therefore only be explained by the loss of $H_2{}^{18}O$ from the precursor.

Fig. 3b shows that the product ion spectrum from the isolation and fragmentation of the primary product ion at *m/z* 163 results in product ions at *m/z* 143, 135, 133, 121, 107, and 91. The ions at *m/z* 135, 121, and 107 must include the ^{18}O oxygen, whereas the ions at *m/z* 143, 133, and 91 must not contain the ^{18}O oxygen. A particularly interesting observation is the distribution of the secondary product ions at *m/z* 135 and *m/z* 133, which highlights competing pathways through the loss of ethylene (C_2H_4) and $C^{18}O$ for the loss of 28 or 30 Da, respectively, from the primary product ion at *m/z* 163 for α-PVP (Fig. 3b). Isolation and fragmentation of the ^{18}O-containing secondary product ion at *m/z* 121 results in only the tropylium ion at *m/z* 91, again consistent with the loss of CO from the precursor with the elemental composition $C_8H_7{}^{18}O^+$ at *m/z* 121.

Fig. 4 contains the MS^n fragmentation of α-PVP that has a ^{13}C label on the α-carbon. Fragmentation of the isotope-labeled precursor ion $[M+H]^+$ at *m/z* 233 (Fig. 4a) results in product ions at *m/z* 162, 144, 134, 127, 120, 105, and 92. These product ions are entirely consistent with the product ions observed in Fig. 2a with the ^{13}C label on the carbonyl carbon instead of the α-carbon. Fig. 4b shows the product ions formed through the isolation and fragmentation of the intermediate at *m/z* 162, which includes *m/z* 144, 134, 120, and 92. Fragmentation of the intermediate ion at *m/z* 120 is almost devoid of signal at *m/z* 91 for the all-^{12}C-isomer (Fig. 4c), which indicates that the α-carbon is retained and the carbonyl carbon is not.

Based on the isotope labeling and MS^n results, Fig. 5 shows the proposed fragmentation mechanisms for the generation of the product ions at *m/z* 134, 133, and 120 from collisional activation of the protonated molecular ion of ^{13}C-carbonyl-α-PVP at *m/z* 233. After the loss of the pyrrolidine moiety from the precursor, the ion at *m/z* 162 follows two primary pathways. The first is the loss of ^{13}CO directly from the alkyl chain, which results in the formation of the intermediate at *m/z* 133 (green pathway). The other dominant pathway for the intermediate at *m/z* 162 is through the formation of an epoxide, which stabilizes the charge on a tertiary carbocation. The epoxide can fragment through a variety of charge-remote mechanisms including a 4-center elimination of ethylene to give the product at *m/z* 134 (red pathway) and through a different 4-center elimination of propylene to give the product at *m/z* 120 (blue pathway). For the precursor labeled with ^{13}C on the carbonyl carbon, the loss of ^{13}CO (29 Da) and the loss of C_2H_4 (28 Da) are readily distinguished. In contrast, the unlabeled precursor provides losses of ^{12}CO (28 Da) and C_2H_4 (28 Da) have the same nominal mass and are indistinguishable on unit-mass-resolution instruments.

According to DFT calculations, there is no energy barrier to form the epoxide at *m/z* 162 in the top right of Fig. 5 from the secondary carbocation in the top center of Fig. 5. The epoxide carbon distal to the

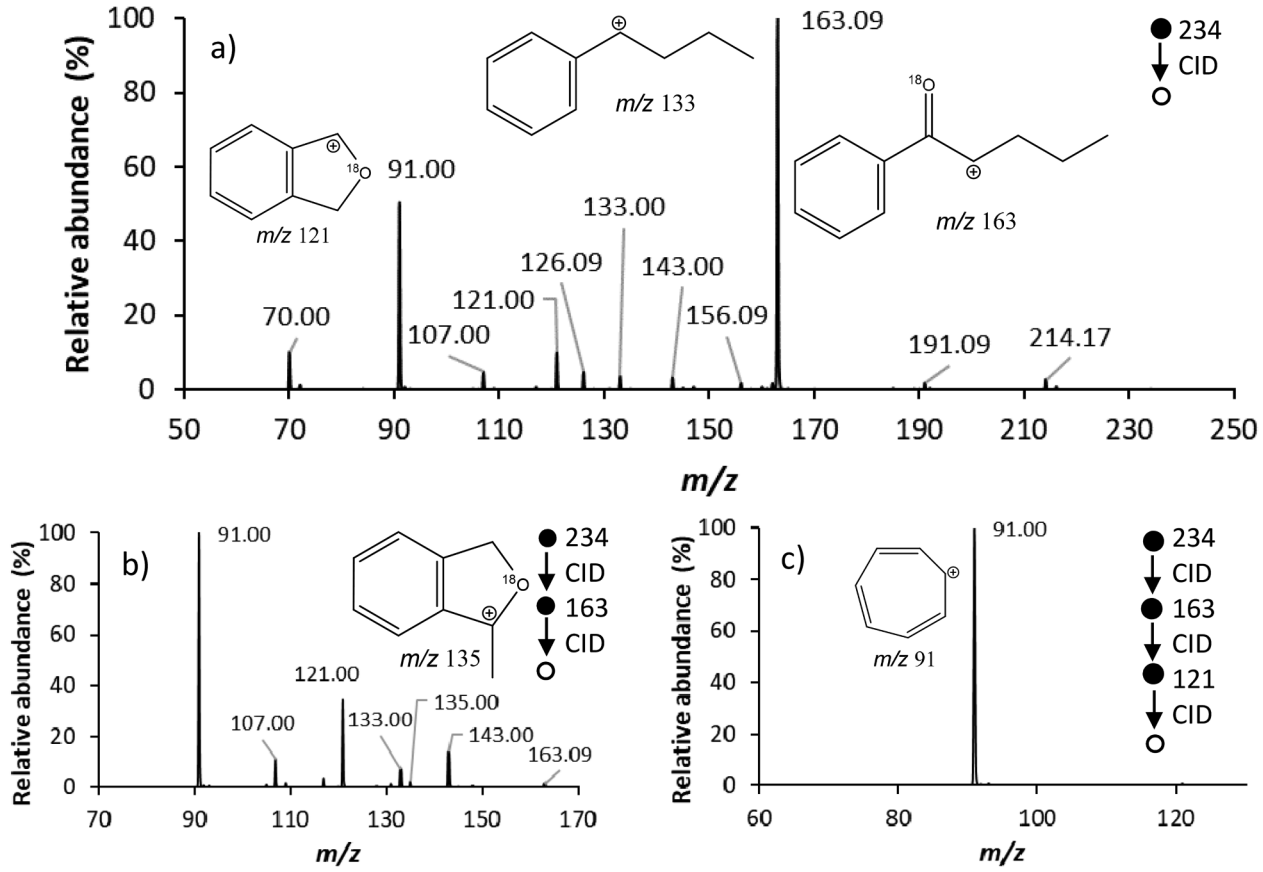

Fig. 3. Tandem mass spectra of ^{18}O-α-PVP: a) MS^2 product ion spectrum of the $[M+H]^+$ molecular ion (35% NCE); b) MS^3 spectrum of the product ion at *m/z* 163 (30% NCE) showing the formation of product ions at *m/z* 143, 135, 133, 121, 107 and 91; c) MS^4 spectrum of the secondary product ion at *m/z* 121 (30% NCE) showing only the formation of tropylium ion at *m/z* 91. Evidence for the phthalane structures in panels a) and b) are provided by ion spectroscopy and DFT calculations in section 3.4.

ring can then undergo nucleophilic attack by π-electrons from the aromatic ring—after or during the loss of an ethylene or propylene neutral loss of 28 or 42 Da, respectively—to provide the phthalane core for the product ions at *m/z* 134 and *m/z* 120, respectively. DFT calculations show that the phthalane structure (bottom right structure in Fig. 5) is thermodynamically the most stable isomer compared to seven alternative isomeric structures. However, energy barriers associated with these isomer interconversions have not been studied. These mechanisms help explain both the presence of the secondary product ions at *m/z* 134 and *m/z* 133, and they are consistent with the ion spectroscopy results for the most probable structures (see below). The competing pathways between the loss of the non-^{13}C-labled ethylene neutral (28 Da) and the ^{13}C-labled CO neutral (29 Da) explains the presence of both *m/z* 134 and *m/z* 133 in the product ion spectrum of ^{13}C-carbonyl carbon-α-PVP (Fig. 2b).

Fig. 6 shows two possible mechanisms for the formation of the product ions at *m/z* 91 and *m/z* 92 from the intermediate at *m/z* 120. The conversion energetics of the last few steps—from the benzylium ion to the tropylium ion—have been described in detail by Vala et al. [49]. These pathways are based on the ^{13}C isotopic labeling of both the carbonyl carbon and α-carbon, and they help explain the observations that the α-carbon is incorporated into the tropylium ion through the loss of neutral CO containing the carbonyl carbon. According to the acquired spectra, the alkyl hydrogens must have a sufficiently high barrier for rearrangement to prevent the phthalane structures at the top of Fig. 6 from interconverting. The two fragments shown at the top of Fig. 6 are therefore distinct and not in equilibrium.

Supplemental Fig. 3a shows the MS^3 product ion spectrum from the intermediate product ion at *m/z* 134 for ^{13}C-carbonyl carbon-α-PVP. This spectrum highlights the formation of product ions at *m/z* 106, 105, and 92. The corresponding MS^3 product ion spectrum for the intermediate product ion at *m/z* 133 for ^{13}C-carbonyl carbon-α-PVP is shown in Supplemental Fig. 3b. Supplemental Fig. 3b demonstrates the formation of product ions at only *m/z* 105 and *m/z* 91. Supplemental Fig. 4 shows the proposed mechanisms for the formation of the *m/z* 106, 105, 92, and 91 product ions from the intermediate product ions at *m/z* 134 and *m/z* 133 for ^{13}C-carbonyl carbon-α-PVP. Supplemental Fig. 5 shows the MS^3 fragmentation of the intermediate product ion at *m/z* 134 from ^{13}C-α-carbon-α-PVP and Supplemental Fig. 6 demonstrates the proposed mechanisms to explain the product ions at *m/z* 106, 105, 92, and 91.

The analysis of α-PVP-d_7, which is perdeuterated along the alkyl chain, provides additional support for the proposed mechanisms shown in Figs. 5 and 6. When α-PVP is perdeuterated along the alkyl chain, the $[M+H]^+$ precursor ion is observed at *m/z* 239, and fragmentation of the d_7 precursor results in abundant fragments at *m/z* 168, 140, 120, 93 and 92, among others (Fig. 7a). Isolation and fragmentation of the intermediate at *m/z* 168 (Fig. 7b) shows an interesting distribution of fragments around *m/z* 92 and *m/z* 120. The formation of the ion at *m/z* 92 must occur through the incorporation of a single deuterium into the tropylium ion, whereas the formation of ions at *m/z* 93 and *m/z* 94 must involve the incorporation of two and three deuteriums, respectively, into the tropylium ion. This same pattern of deuterium inclusion is observed for the intermediates at *m/z* 120, 121, and 122. The mechanims described in Figs. 5 and 6 are consistent with the experimental observations regarding scrambling along the alkyl chain (*m/z* 93 and *m/z* 121) and the aromatic ring (*m/z* 94 and *m/z* 122).

Based on the results for the fragmentation of α-PVP labeled with

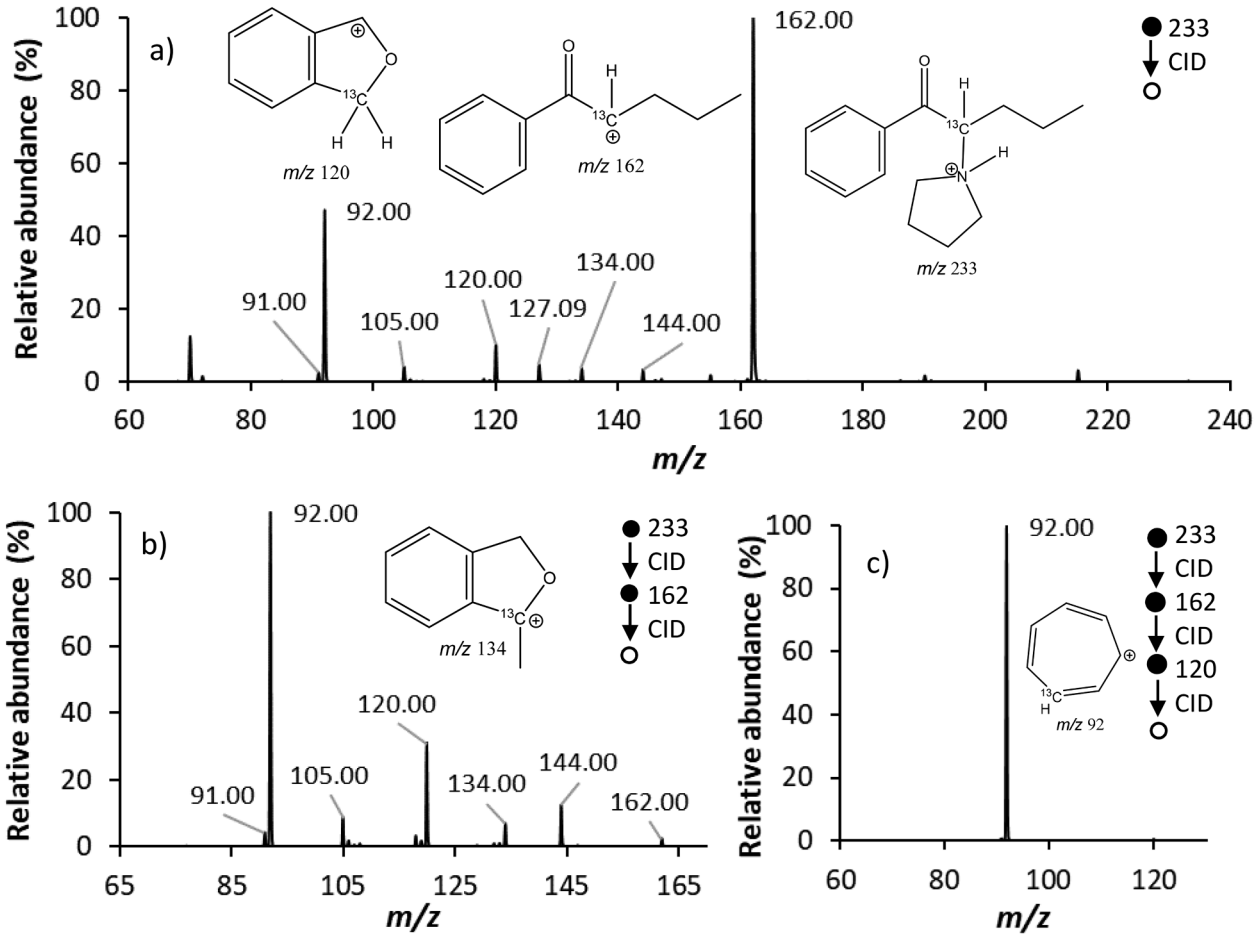

Fig. 4. Tandem mass spectra of ^{13}C-α-carbon α-PVP: a) MS^2 product ion spectrum of the $[M+H]^+$ molecular ion (35% NCE); b) MS^3 spectrum of the intermediate ion at *m/z* 162 (30% NCE); c) MS^4 spectrum of the intermediate ion at *m/z* 120 (30% NCE) showing the formation of only the product ion at *m/z* 92. Evidence for the phthalane structures in panels a) and b) are provided by ion spectroscopy and DFT calculations in section 3.4.

^{18}O, one would expect α-PVP-d_7 to lose either ^{12}CO (28 Da) or C_2D_4 (32 Da) from the intermediate at *m/z* 168 to provide product ions at *m/z* 140 and *m/z* 136, respectively. Although both are observed, only the intermediate product ion a *m/z* 140 is readily observed in the full-scale plot. These observations are consistent with both the $C_9H_9O^+$ and $C_{10}H_{13}^+$ intermediate product ions in unlabeled α-PVP, which are discussed later in the high-resolution mass spectrometry section.

ESI-MS/MS analysis of other cathinone structures showed that the alkyl chain length has a direct impact on the formation of the tropylium ion and associated intermediate product ions. As the alkyl chain length increases, additional intermediates are possible, and they also contribute to the formation of the tropylium ion. For example, PV8 has two additional methylene groups relative to α-PVP. The $[M+H]^+$ precursor of PV8 is observed at *m/z* 260, and the major product ions appear at *m/z* 189, 147, 133, 119 and 91. Consistent with the other pyrrolidine-containing cathinones, the structure of the intermediate product ion at *m/z* 189 corresponds to the preferred loss of the pyrrolidine ring from the precursor. The structure of the intermediate product ion at *m/z* 119 is presumably the same as in Fig. 1, which likely has the same phthalane structure as shown in Figs. 1 and 5. The mass of the intermediate product ion at *m/z* 147 suggests that it corresponds to the fragment at *m/z* 133 (described in Figs. 2, 3 and 5) with an additional methylene group (CH_2). Secondary fragmentation of the intermediate at *m/z* 147 provides secondary product ions at *m/z* 119 and *m/z* 91.

Product ion spectra change more dramatically when the alkyl chain length is decreased relative to α-PVP. For example, Supplemental Fig. 7 shows ESI-MS/MS spectra of cathinones with both shorter and branched alkyl chains and their ability to prevent the formation of the tropylium ion. Our results show that when the alkyl chain attached to the aromatic ring is at least four carbons long (including the carbonyl cabon), the tropylium ion is observed, which is consistent with previous results [18,22,37,50]. However, as a general rule, when the alkyl chain is shorter than four carbon atoms, the formation of the tropylium ion is severely inhibited. These observations are explained by the need for a sufficient number of carbons on the alkyl appendage to enable both sterically favorable rearrangements and a good leaving group for the phthalane ring to form, as is the case for α-PVP in Fig. 5. Finally, Supplemental Fig. 7 shows that even when the alkyl chain contains four carbon atoms, the incorporation of a methyl group on the α-carbon also quenches the mechanism for tropylium ion formation. Quenching of the tropylium ion formation is an expected outcome of the mechanism shown in Fig. 5 because the additional methyl group on the α-carbon both stabilizes the charge on the α-carbon and provides steric hinderance to the nucleophilic attack by the π-electrons from the aromatic ring.

Fig. 8 shows the ESI-MS/MS spectrum of protonated 3,4-MDPV-d_8. The spectrum indicates that the deuterium atoms on the pyrrolidine ring are not incorporated into the benzene ring during the skeletal rearrangement and instead remain on the pyrrolidine moiety. The absence of deuterium scrambling is confirmed with the product ion at *m/z* 134, which is an 8 Da mass increase relative to the 1-butylidene-pyrrolidin-1-ium product ion at *m/z* 126 observed for non-deuterated 3,4-MDPV (Fig. 8a). When the $[M+H]^+$ precursor of 3,4-MDPV-d_8 at *m/z* 284 is isolated and fragmented, the base peak is the secondary product ion at *m/z* 205 (Fig. 8a). This ion is a 44 Da mass increase relative to the secondary product ion at *m/z* 161 of α-PVP, which

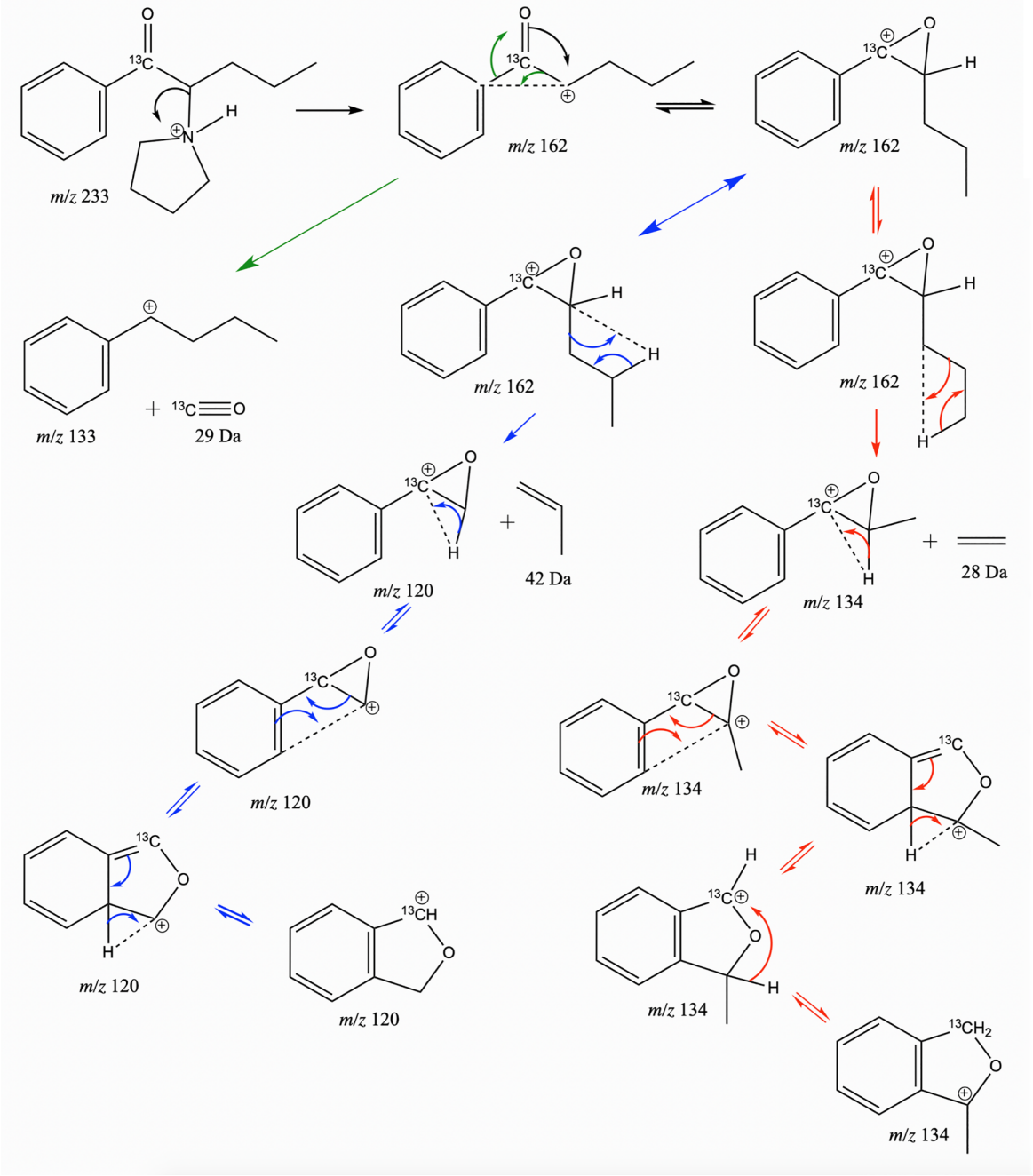

Fig. 5. Proposed mechanisms for the formation of *m/z* 134, 133, and 120 product ions from ^{13}C-carbonyl carbon-α-PVP. The phthalane structures at *m/z* 120 and *m/z* 134 were confirmed by ion spectroscopy and DFT calculations (see Figs. 12 and 13).

corresponds to the additional mass of the methylenedioxy substituent, as expected.

MS^3 fragmentation of the base peak at *m/z* 205 for 3,4-MDPV-d_8 produces secondary product ions at both *m/z* 177 and *m/z* 163, which both represent a 44 Da mass increase relative to the corresponding non-methylenedioxy substitutions observed for α-PVP (Fig. 8b). These fragments also support the conserved nature of the proposed fragmentation mechanisms that are apparently unperturbed by modifications on the aromatic ring. The product ion at *m/z* 175 forms through the loss of formaldehyde (CH_2O), which comes from the methylenedioxy substituent and explains why this equivalent fragment is not observed for α-PVP. Fig. 8c shows the isolation and fragmentation of the intermediate product ion at *m/z* 177 for 3,4-MDPV-d_8, which highlights the loss of both propylene (42 Da) and formaldehyde (30 Da). Again, the formaldehyde loss from 3,4-MDPV comes from the methylenedioxy substituent, which is not present for α-PVP.

Supplemental Fig. 8 compares the tandem mass spectra of the $[M+H]^+$ precursor ion for 3,4-MDPV and the $[M+H]^+$ precursor ion for 2,3-MDPV, both of which are observed at *m/z* 276. In both cases, the major fragments leading to the formation of the substituted tropylium ions are observed at *m/z* 205, 177, 163 and 135. However, the isomers have different fragment ion abundances at *m/z* 205 and *m/z* 135. When the methylenedioxy substituent is in the 3,4-positon, the intermediate product ion at *m/z* 205 is the base peak of the tandem mass spectrum and the product ion at *m/z* 135 is present at ~10% abundance. In contrast, when the methylenedioxy substituent is in the 2,3-position, the intermediate product ion at *m/z* 205 is only about 40% of the base peak and the product ion at *m/z* 135 is about 70% of the base peak. This

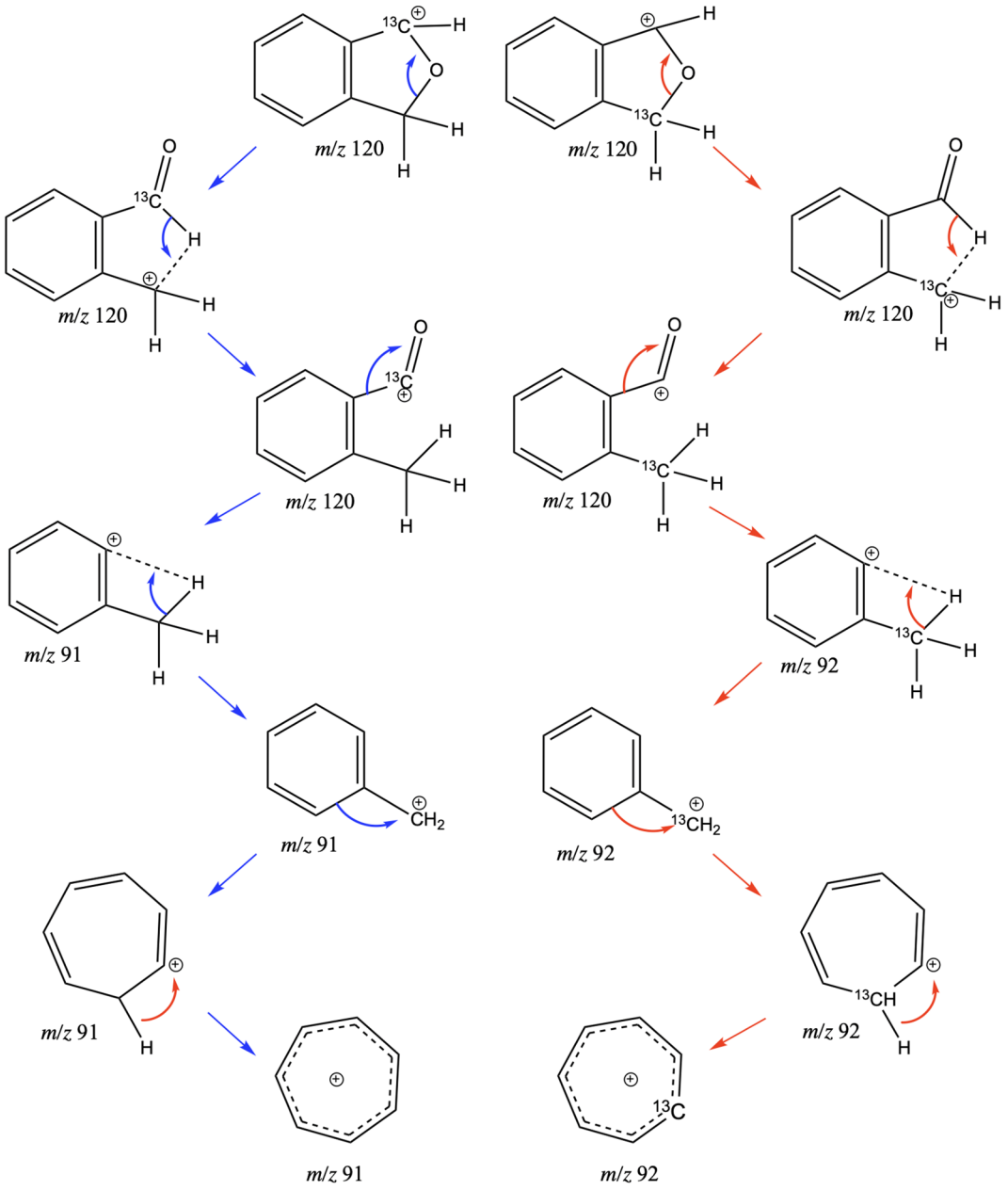

Fig. 6. Proposed mechanisms for the formation of product ions at *m/z* 91 and *m/z* 92 from the intermediate at *m/z* 120 for MS^4 based on ^{13}C isotopic labeling of the carbonyl carbon and the α-carbon for α-PVP.

behavior highlights two trends about the position of the methylenedioxy substituent: 1) the formation of the tropylium ion is favored for the 2,3-position, and 2) the loss of formaldehyde from the intermediate product ion *m/z* 205 is favored for the 2,3-positon.

Fig. 9 shows the pathways from the $[M+H]^+$ precursor to the final tropylium product ion along each major pathway for α-PBP, α-PVP, and PV8. The flux is expressed as a percentage of the total ion spectrum. As discussed previously, when the alkyl chain length increases there are additional intermediate product ions that feed into the tropylium ion pathway. Likewise, the conversion rate from precursor to intermediate changes as a function of possible pathways, where α-PBP contains only two intermediates and PV8 contains four intermediates along the tropylium ion pathways. The length of the alkyl chain has a direct effect on the conversion rates; the intermediate product ion at *m/z* 133 for α-PVP having a 79% conversion to the tropylium product ion at *m/z* 91, whereas the intermediate product ion at *m/z* 133 from PV8 has only a 1% conversion rate to the tropylium product ion at *m/z* 91. Fig. 9 also shows that the conversion rate for the intermediate product ion at *m/z* 119 to the tropylium product ion at *m/z* 91 is ~ 100% for the three unsubstituted cathinones.

3.2. High-Resolution mass spectrometry (HRMS) measurements using ESI-Q-TOF

Whereas the IT mass spectrometer offered the capability to perform multiple stages of mass spectrometry (MS^n), HRMS allowed for accurate mass measurements from the tandem mass spectra. Accurate mass measurements are useful because they provide unique elemental compositions, with our typical instrument uncertainty on the order of 10 ppm or about 3 mDa. The ability to identify the elemental composition of a fragment becomes particularly important when there are multiple ways to explain a neutral loss, such as CO and C_2H_4, which

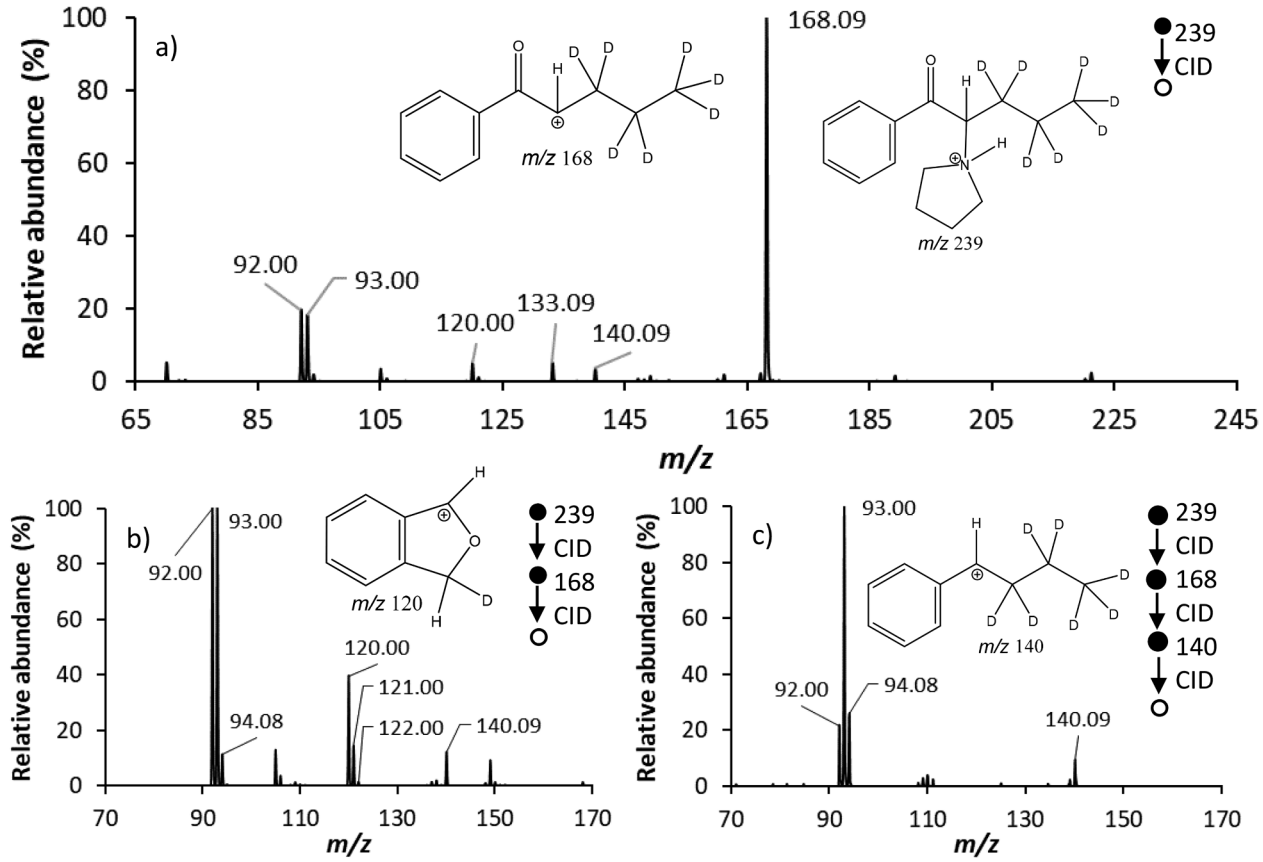

Fig. 7. Tandem mass spectra of α-PVP-d_7: a) MS^2 product ion spectrum of the $[M+H]^+$ molecular ion (35% NCE); b) MS^3 product ion spectrum of the product ion at *m/z* 168 (30% NCE) showing the formation of secondary product ions at *m/z* 140, 122, 121, 120, 94, 93, and 92; c) MS^4 product ion spectrum of the intermediate at *m/z* 140 (30% NCE) showing the formation of secondary product ions at *m/z* 92, 93, and 94.

both have the nominal mass of 28 Da. Fig. 10a shows the high-resolution tandem mass spectra of α-PVP with the major structural fragments embedded.

The HRMS tandem mass spectrum of α-PVP allows for the determination of the elemental formula of four important ions. The first is the tropylium ion with an accurate mass of *m/z* 91.0559, which is about 12 ppm from the exact mass of $C_7H_7^+$. The second important ion is the proposed phthalane structure with an accurate mass of *m/z* 119.0530, which deviates 28 ppm from the exact mass for $C_8H_7O^+$. Finally, the HRMS measurements of the two product ions with a nominal mass of *m/z* 133 in Fig. 10a had elemental compositions of both $C_9H_9O^+$ (measured at *m/z* 133.0670; expected at *m/z* 133.0653; 13 ppm error) and $C_{10}H_{13}^+$ (measured at *m/z* 133.1029; expected at *m/z* 133.1017; 9 ppm error). Beam-type CID in the HRMS instrument tends to favor the formation of fragments at smaller *m/z* values than in the lower-energy IT instrument, as shown by the low-abundance $C_{10}H_{13}^+$ product ion relative to the $C_9H_9O^+$ product ion under 35 eV CID conditions (Fig. 10b). The slight differences in the accurate mass measurements in Fig. 10a and 10b are because the zoomed-in plot in Fig. 10b was collected at a collision energy of 35 eV; the differences in accurate mass are representative of the typical uncertainty in replicate measurements. The combination of the ^{18}O-α-PVP IT results (Fig. 3) and the HRMS results provide unequivocal evidence for the competing pathways between the loss of CO and ethylene for the formation of the product ion with a nominal mass of *m/z* 133.

Fig. 11 shows the tandem mass spectra of PV8 with the major structural fragments embedded. Although the alkyl chain is two carbons longer for PV8 than α-PVP, the same core tropylium ion fragmentation ions are observed for both α-PVP and PV8. Based on the HRMS accurate mass measurements, the error between the accurate mass measurements and exact masses is on the order of those discussed in Fig. 10. The additional intermediate at *m/z* 147.0838 is hardly above the noise level at the conditions used for this experiment; however, the accurate mass measurement is consistent with the elemental formula $C_{10}H_{11}O^+$. Supplemental Fig. 9 contains an additional example of the tandem mass spectra generated with the Q-TOF mass spectrometer for 3,4-MDPV.

3.3. General fragmentation trends and practical implications

Based on the accurate mass measurements from the Q-TOF mass spectrometer and the MS^n fragmentation from the IT mass spectrometer, the following generalized trends can be made about the fragmentation behavior of α-pyrrolidinophenone synthetic cathinones. Unlike *N*-alkylated synthetic cathinones [36,37], radical fragments are rarely formed from the even-electron precursors. The loss of the 71 Da pyrrolidine neutral is always observed, as shown by the product ion at *m/z* 189 for PV8. From this intermediate, there are competing pathways for the loss of CO and ethylene (both nominally 28 Da), and the loss of CO is favored for all the studied compounds. For the model compound PV8, these two elementally distinct product ions both occur at the same nominal *m/z* value of 161. Any member of this class of cathinones with a carbon skeleton comprised of at least four contiguous carbon atoms, including the carbonyl carbon, can form products through the loss of neutral alkenes from the aliphatic chain. For the model compound PV8, two such products are observed at *m/z* 133 for the loss of 28 Da (C_2H_4) from the intermediate at *m/z* 161 and *m/z* 147 for the loss of 42 Da (C_3H_6) from the intermediate at *m/z* 189. The intermediate formed through the loss of propylene feeds directly into the tropylium ion pathway through the loss of 28 Da (ethylene) in all cases studied, as shown by the product ion at *m/z* 119 for all cathinones. The intermediate at *m/z* 119 forms the tropylium ion at *m/z* 91 through the loss of CO for all the studied α-pyrrolidinophenone cathinones. Finally, the

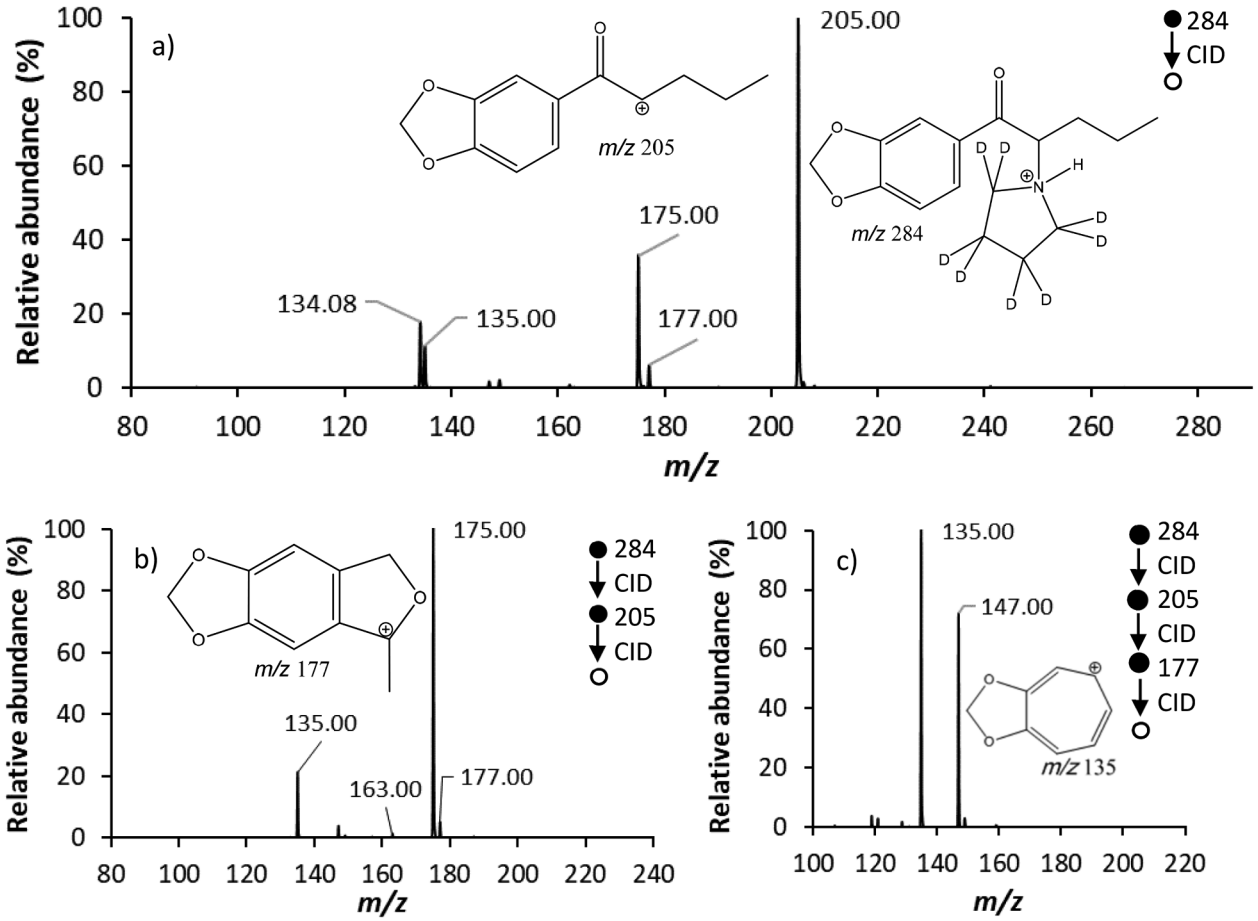

Fig. 8. Tandem mass spectra of 3,4-MDPV-d_8: a) MS^2 product ion spectrum of the $[M+H]^+$ molecular ion (35% NCE); b) MS^3 product ion spectrum of the product ion at *m/z* 205 (35% NCE) showing the formation of secondary product ions at *m/z* 177, 163 and 135; and c) MS^4 product ion spectrum of the product ion at *m/z* 177 (35% NCE) showing the formation of the tropylium ion derivative at *m/z* 135.

intermediate at *m/z* 133 forms the tropylium ion through the loss of C_2H_2O, as shown in Supplemental Fig. 4 for ^{13}C-carbonyl carbon-α-PVP.

The differences in the mass spectra generated with IT and Q-TOF mass spectrometers are beyond the focus of the current project. However, in brief, the IT mass spectrometer favors the formation of lower energy and higher mass intermediate ions relative to the Q-TOF mass spectrometer, which included some higher-energy pathways like the loss of alkyl radicals to form odd-electron product ions. These spectral differences stem from the well-known differences in the collision energy, number of collisions, and activation time scales between the IT and Q-TOF mass spectrometers. IT fragmentation involves trapping CID (very slow activation, i.e. 10–100 ms) through hundreds of collisions with the bath gas, whereas Q-TOF fragmentation occurs through low-energy (slow activation, i.e. 0.5–1 ms) beam-type collisions (i.e. 10–100) as the analyte passes through the collision cell [51,52].

In general, the mass spectra collected with both the IT and Q-TOF mass spectrometers were sufficiently similar that they are cross-comparable, and the fragmentation pathways were conserved across all synthetic cathinones analyzed. The impact of this information is that it allows for a quick and easy manner for the detection of aromatic substitutions on synthetic cathinones. In contrast to typical tandem mass spectra, a dominant peak for this class of cathinones at nominal *m/z* 91 indicates an unsubstituted aromatic ring, a peak at nominal *m/z* 105 indicates a methyl-substituted aromatic ring (Supplemental Fig. 10), and a peak at nominal *m/z* 135 indicates a methylenedioxy substitution. Any isotope labels on the carbonyl carbon or oxygen should not affect the *m/z* positions of these substituted tropylium ions.

3.4. Infrared ion spectroscopy

The combination of the MS^n and accurate mass measurement results determined the relationship between each intermediate product ion of interest and the tropylium ion, but also the elemental formula of those intermediates. However, neither of these techniques allow for the determination of the exact arrangement of the atoms present in each intermediate. To help answer the question of constitutional arrangement, gas-phase infrared ion spectroscopy was employed to characterize the intermediates at *m/z* 119 and *m/z* 133 for α-PVP.

Fig. 12 shows a comparison between the experimentally observed gas-phase IR spectra and the theoretically calculated DFT spectra for two proposed structures for the intermediate product ion at *m/z* 119. Based on being the lowest-energy isomer from eight isomeric structures evaluated (Supplemental Fig. 1), and the similarity in wavenumber between the experimental and theoretical calculation, the structure labeled 119a was identified as the most likely structure for the intermediate product ion at *m/z* 119. We note here that the IR-induced dissociation was energetically demanding, requiring 10 FEL pulses at high IR laser pulse energy, probably as a consequence of the compact nature of the interrogated structures. We suspect these high thresholds in combination with non-linearities in the multiple-photon excitation process lead to a skewed frequency dependence of the fragment yield, reducing the observed intensities in the IRMPD spectra towards lower photon energies.

The structure 119d is an example of a poor fit both in terms of relative energy of formation (208 kJ/mol relative to structure 119a) and alignment of the experimental and theoretical spectra. The principal feature of the calculated spectra of 119d at ~1850 cm^{-1} can be

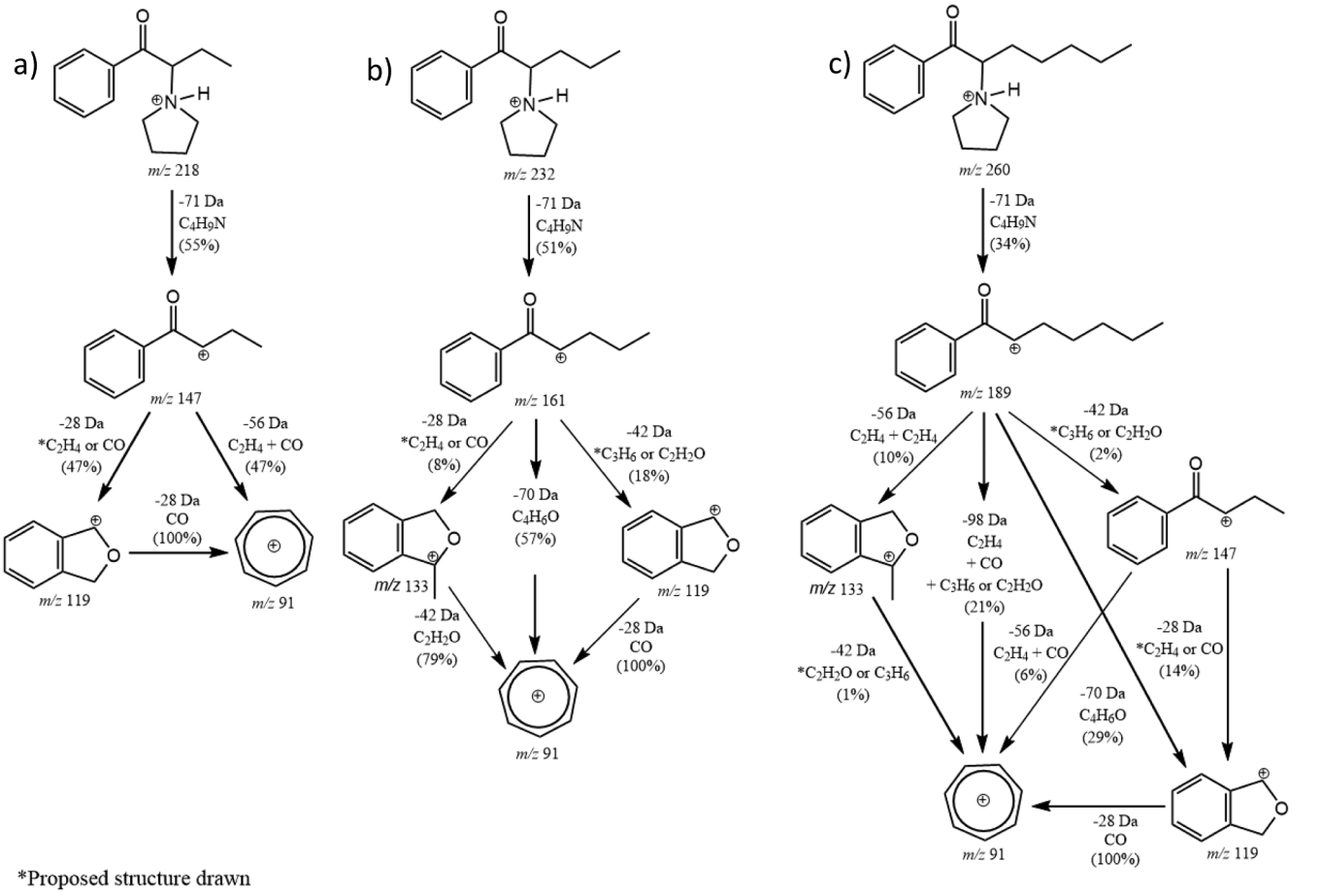

Fig. 9. Selected fragmentation pathways and corresponding flux for: a) α-PBP, b) α-PVP, and c) PV8. The percentages shown at each level of MS^n provide the ion's abundance relative to the summed ion abundance of the product ion spectrum at that level. For example, *m/z* 147 is the base peak (100% peak height) in the MS^2 product ion spectrum of α-PBP and 55% of the summed product ion spectrum.

assigned to the stretching of the carbonyl bond. The highly coupled stretch of the Cα–Cβ bonds is responsible for both the peaks at ~1600 cm^{-1} and 1400 cm^{-1}. Based on the experimental spectra, we know that the intermediate product ion at *m/z* 119 cannot contain a carbonyl because of the absence of the characteristic feature at 1850 cm^{-1}, which is well beyond the experimentally observed peak at 1600 cm^{-1}. The additional peaks in the measured spectrum between ~1100–1500 cm^{-1} derive from C-H wagging of CH_2 hydrogens. The absence of the feature at the carboxylic absorption wavelength and the good match of the peak at ~1600 cm^{-1}, assigned to a highly-coupled C–C stretching of aromatic carbon bonds, along with the most favorable thermodynamics, make isomer 119a the most probable structure of the *m/z* 119 fragment.

Fig. 13 shows the analogous comparison for the intermediate product ion at *m/z* 133. The 133a' structure was identified as the most likely structure for the intermediate product ion at *m/z* 133 based on the relative energy (35 kJ/mol more stable than the next isomer Supplemental Fig. 2) and similarity between the experimental and theoretical spectra. The experimental band at ~1600 cm^{-1} matches well with the theoretical absorption frequency for a highly-coupled C–C stretching mode involving all aromatic carbons and C(aromatic)–Cα bonds. The experimental absorption at ~1500 cm^{-1} is matched by Cα–Cβ and Cα–O stretching coupled to aromatic C–H wagging. The absorption at ~1400 cm^{-1} is where CH_2 and CH_3 scissoring motions are predicted to absorb. In comparison, structure 133c gives a poorer fit because of the high relative energy (123 kJ/mol) and the significant differences between the experimental and theoretical spectra. For instance, the main predicted band, the C═O stretch coupled to adjacent C–C stretching modes, should appear near 1700 cm^{-1}, but is absent in the experimental IRMPD spectrum. Thus, the IR spectra indicate that neither an epoxide nor a carbonyl functional group are abundant in the ions at *m/z* 119 or *m/z* 133.

The gas-phase IR spectra in Fig. 13 indicates the presence of two structures in the IR spectra. The structure 133a' has both the best spectral match and the lowest energy configuration and is likely the dominant structure. However, the structure 133 g, which lacks an oxygen, cannot be ruled out and is also likely to be present. The MS^n and accurate mass data indicate the loss of the CO is favored over the loss of ethylene (C_2H_4) for α-PVP. However, the accurate mass data indicates that both pathways co-exist, so both structures are likely to be present in the gas-phase ion spectroscopy analysis. Due to the isobaric nature of these compounds, the isolation step before IR irradiation of the ions is unable to separate the intermediates $C_9H_9O^+$ and $C_{10}H_{13}^+$ that are both observed at nominal *m/z* 133.

The various experiments described above enable the generation of a general set of rules to describe the fragmentation patterns and the formation of substituted tropylium ions in the tandem mass spectra of substituted cathinones. For example, the base peak in the tandem mass spectra of most α-pyrrolidine-containing cathinones stems from the neutral loss of the pyrrolidine moiety. The only exception in our studies was 2,3-MDPV. The second common feature in the fragmentation behavior is the competition between the loss of CO and ethylene (C_2H_4) from this base peak, which both have a nominal mass of 28 Da. Of the two losses, the loss of CO is typically dominant.

Another experimentally observed aspect of the fragmentation behavior is that competing fragmentation pathways lead to the formation

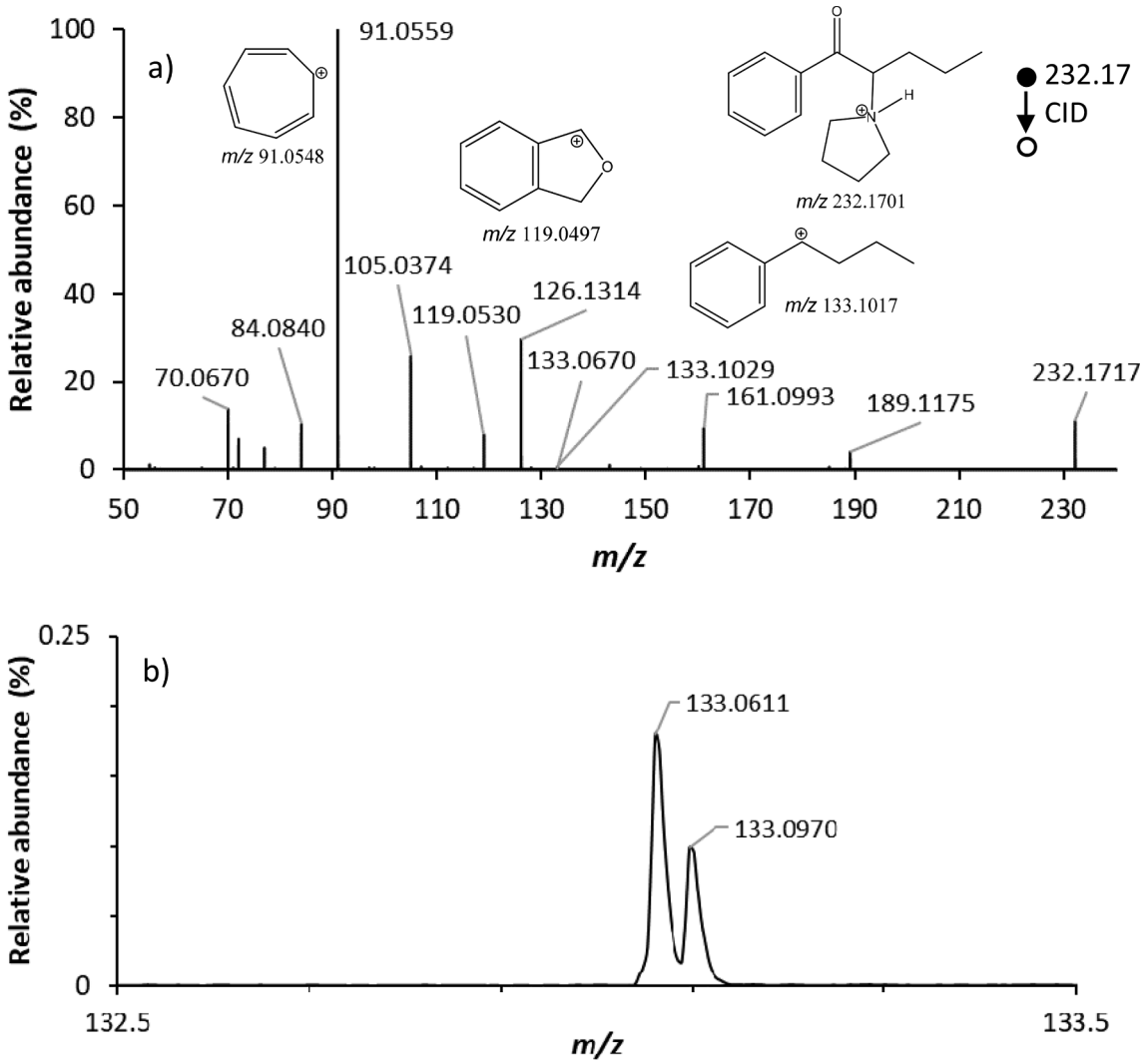

Fig. 10. Tandem mass spectra of α-PVP showing: a) the fragmentation observed on the Q-TOF mass spectrometer with a 25 eV collision energy and b) a zoomed-in view of the product ions at *m/z* 133.0611 and *m/z* 133.0970 with a slightly higher collision energy of 35 eV.

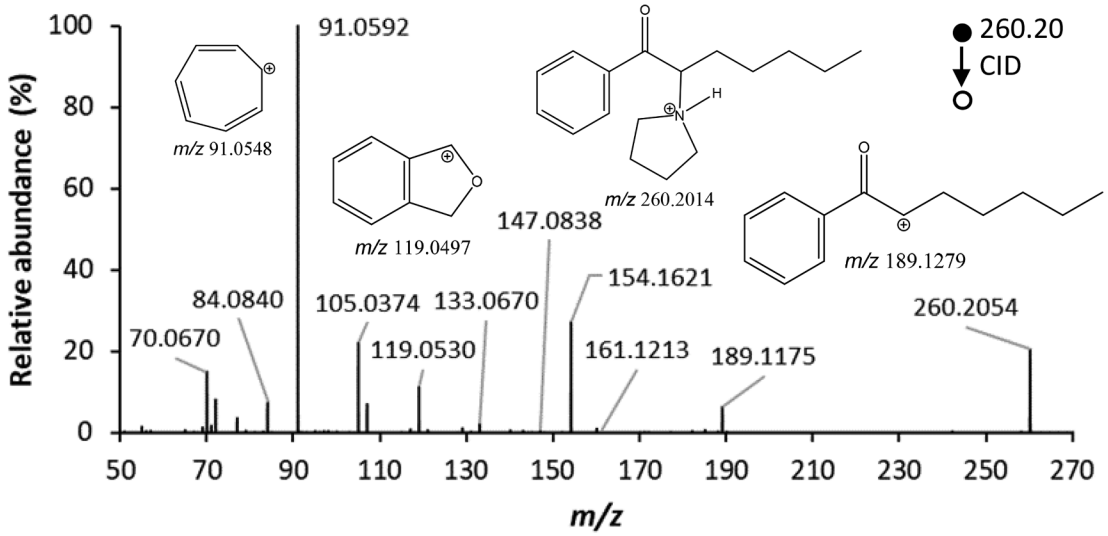

Fig. 11. Tandem mass spectra of PV8 (25 eV) showing the conserved nature of the loss of the pyrrolidine moiety with the Q-TOF mass spectrometer and the propensity to form the tropylium ion.

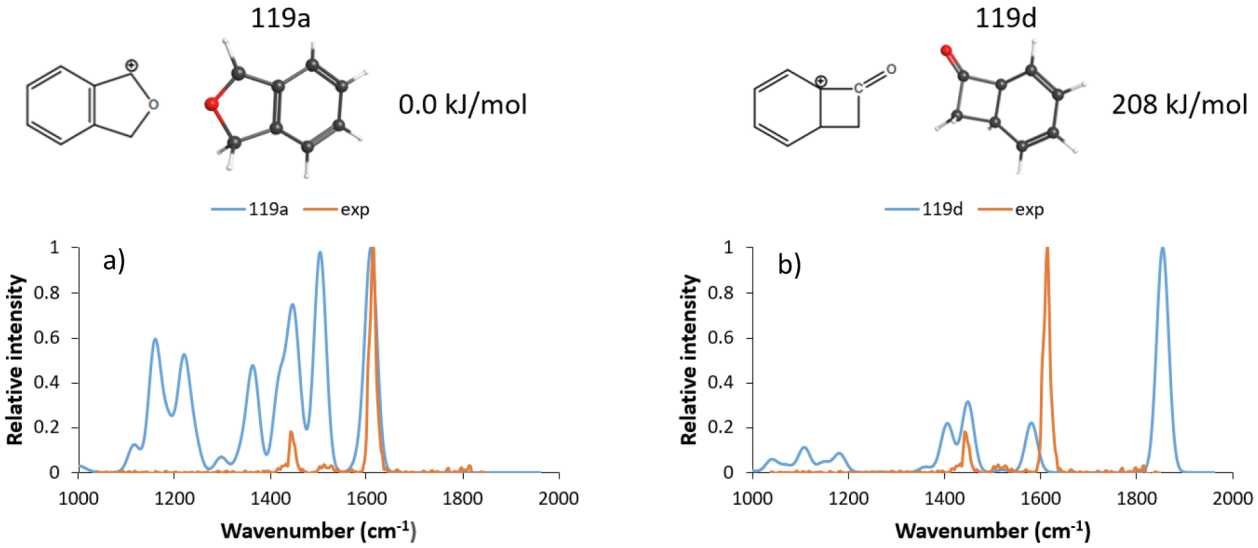

Fig. 12. Comparison of experimental gas-phase IR ion spectroscopy and DFT theoretical IR spectra for fragments of protonated α-PVP: a) proposed 119a structure demonstrating a good alignment between experimental and predicted spectra and b) proposed 119d structure demonstrating a poor alignment between the experimental and predicted spectra.

of the tropylium ion via various neutral losses from the alkyl chain. As far as we have established, the fragmentation pathways seem to go through one of two phthalane structures shown in Fig. 5; the only difference between the two is whether or not there is a methyl substitution on the saturated phthalane ring. The use of ^{13}C isotopic labeling on both the carbonyl carbon and α-carbon demonstrate that the α-carbon from the *m/z* 120 intermediate ion is almost exclusively incorporated into the tropylium ion and the carbonyl carbon is quantitatively lost as neutral CO, which, to our knowledge, has not been demonstrated in literature before.

There are several requirements for the proposed tropylium ion rearrangements to occur. First, the alkyl chain must be at least four carbon atoms long (including the carbonyl carbon) to enable the necessary rearrangements to occur. Second, there must be a reasonable leaving group available prior to ring expansion. Third, the α-carbon must not be substituted; in the case of methyl substitution on the α-carbon, for example, the methyl group poses a barrier to nucleophilic attack and the bicyclic phthalane intermediate cannot form. A final trend in tropylium ion behavior is that the abundance of the tropylium ion tends to increase with increasing alkyl chain lengths. Presumably, longer alkyl chains provide additional pathways towards the tropylium ion and larger alkyl chains provide more stable leaving groups.

Regarding other trends in fragmentation behavior, the mechanisms described in Fig. 5 remain conserved even with additional substituents. For example, the intermediate products ions of 3,4-MDPV show a similar distribution to α-PVP, but shifted by the expected 44 Da of the methylenedioxy substituent. Similarly, when a methyl group is present on the aromatic ring, such as with MPHP, the substituted tropylium ion at *m/z* 105 ($C_8H_9^+$) is more abundant than the native/unsubstituted tropylium ion at *m/z* 91. However, for cathinones with different substituents on the aromatic ring, the favorability of a specific pathway can be influenced by the position of the substituent, as demonstrated for 3,4-MDPV versus 2,3-MDPV. Finally, whereas the proposed mechanisms in Fig. 5 do not pinpoint the exact hydrogens involved in the

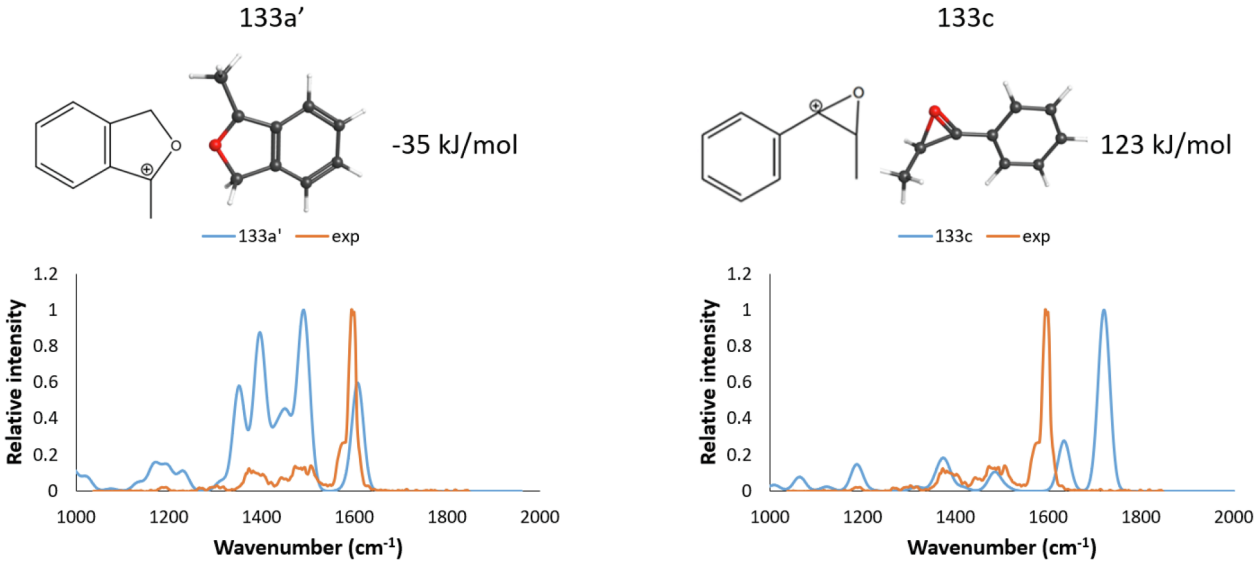

Fig. 13. Comparison of experimental gas-phase IR ion spectroscopy and DFT calculated IR spectra for fragments of protonated α-PVP: a) proposed 133a' structure demonstrating a good alignment between experimental and predicted spectra and b) proposed 133c structure demonstrating a poor alignment between the experimental and predicted spectra.

hydride shifts, the iminium-d_8 product ion at m/z 134 of deuterated 3,4-MDPV-d_8 specifically exclude the hydrogens on the pyrrolidine ring. In this class of cathinones the pyrrolidine neutral is lost before any hydrogen rearrangements occur.

4. Conclusions

This manuscript describes the use of MS^n on an IT mass spectrometer, accurate mass measurements with HRMS, stable isotope labeling, and gas-phase infrared ion spectroscopy to elucidate the mechanism of formation of the tropylium ion in the tandem mass spectra of various α-pyrrolidinophenone synthetic cathinones. The identification of the proposed carbon backbone rearrangements for the generation of the tropylium ion or substituted tropylium ion analogs with ESI-MS/MS provides the forensic science community with a mechanistic explanation for this previously unexplained phenomenon. The conserved nature of the proposed mechanisms offers an additional tool for the identification of emerging synthetic cathinones using tandem mass spectra. For example, a ring-substituted α-pyrrolidinophenone synthetic cathinone will typically provide a peak of reasonable abundance that corresponds to the ring-substituted tropylium ion. However, the mechanism requires a good leaving group for the nitrogen atom—such as the pyrrolidine ring—and at least four carbon atoms on the alkylphenone chain (including the carbonyl carbon). Finally, the ability to defend the observations of existing casework and better predict the fragmentation patterns of future synthetic cathinones provides analysts with increased confidence in their interpretations and provides a stronger scientific foundation for their opinions in court.

Declaration of Competing Interest

The authors declare that they have no known competing financial interests or personal relationships that could have appeared to influence the work reported in this paper.

Acknowledgements

This project was supported by grant number 2018-75-CX-0033, awarded by the National Institute of Justice, Office of Justice Programs, and U.S. Department of Justice. The opinions, findings, and conclusions or recommendations expressed in this publication are those of the authors and do not necessarily reflect the views of the Department of Justice. We gratefully acknowledge the Nederlandse Organisatie voor Wetenschappelijk Onderzoek (NWO) for the support of the FELIX Laboratory.

Appendix A. Supplementary data

Supplementary data to this article can be found online at https://doi.org/10.1016/j.forc.2020.100245.

References

[1] M.J. Valente, P. Guedes de Pinho, M. de Lourdes Bastos, F. Carvalho, M. Carvalho, Khat and synthetic cathinones: a review, Arch. Toxicol. 88 (1) (2014) 15–45, https://doi.org/10.1007/s00204-013-1163-9.
[2] K. Zaitsu, M. Katagi, M. Tatsuno, T. Sato, H. Tsuchihashi, K. Suzuki, Recently abused β-keto derivatives of 3,4-methylenedioxyphenylalkylamines: a review of their metabolisms and toxicological analysis, Forensic Toxicol. 29 (2) (2011) 73–84, https://doi.org/10.1007/s11419-011-0111-8.
[3] A.L. Bretteville-Jensen, S.S. Tuv, O.R. Bilgrei, B. Field, L. Bachs, Synthetic cannabinoids and cathinones: prevalence and markets, Forensic Sci. Rev. 25 (2013) 7–26.
[4] J.A. Fass, A.D. Fass, A.S. Garcia, Synthetic cathinones (bath salts): legal status and patterns of abuse, Ann. Pharmacother. 46 (3) (2012) 436–441, https://doi.org/10.1345/aph.1Q628.
[5] P. Griffiths, D. Lopez, R. Sedefov, A. Gallegos, B. Hughes, A. Noor, L. Royuela, Khat use and monitoring drug use in Europe: the current situation and issues for the future, J. Ethnopharmacol. 132 (3) (2010) 578–583, https://doi.org/10.1016/j.jep.2010.04.046.
[6] E.E. Balint, G. Falkay, G.A. Balint, Khat - a controversial plant, Wien. Klin. Wochenschr. 121 (2009) 604–614, https://doi.org/10.1007/s00508-009-1259-7.
[7] J.P. Kelly, Cathinone derivatives: a review of their chemistry, pharmacology and toxicology, Drug Test. Anal. 3 (2011) 439–453, https://doi.org/10.1002/dta.313.
[8] M. Coppola, R. Mondola, Synthetic cathinones: chemistry, pharmacology and toxicology of a new class of designer drugs of abuse marketed as “bath salts” or “plant food”, Toxicol. Lett. 211 (2) (2012) 144–149, https://doi.org/10.1016/j.toxlet.2012.03.009.
[9] P.I. Dargan, R. Sedefov, A. Gallegos, D.M. Wood, The pharmacology and toxicology of the synthetic cathinone mephedrone (4-methylmethcathinone), Drug Test. Anal. 3 (7–8) (2011) 454–463, https://doi.org/10.1002/dta.312.
[10] J. Jerry, G. Collins, D. Streem, Synthetic legal intoxicating drugs: the emerging 'incense' and 'bath salt' phenomenon, Cleve. Clin. J. Med. 79 (4) (2012) 258–264, https://doi.org/10.3949/ccjm.79a.11147.
[11] T.A. Dal Carson, R. Young, R.A. Glennon, Cathinone: An Investigation of Several N-Alkyl and Methylenedioxy-Substituted Analogs, Pharmacol. Biochem. Behav. 58 (4) (1997) 1109–1116.
[12] F. Westphal, T. Junge, P. Rosner, G. Fritschi, B. Klein, U. Girreser, Mass spectral and NMR spectral data of two new designer drugs with an alpha-aminophenone structure: 4'-methyl-alpha-pyrrolidinohexanophenone and 4'-methyl-alpha-pyrrolidinobutyrophenone, Forensic Sci. Int. 169 (2007) 32–42, https://doi.org/10.1016/j.forsciint.2006.07.024.
[13] A. Namera, M. Kawamura, A. Nakamoto, T. Saito, M. Nagao, Comprehensive review of the detection methods for synthetic cannabinoids and cathinones, Forensic Toxicol. 33 (2) (2015) 175–194, https://doi.org/10.1007/s11419-015-0270-0.
[14] Y. Abiedalla, K. Abdel-Hay, J. DeRuiter, C.R. Clark, Differentiation of cyclic tertiary amine cathinone derivatives by product ion electron ionization mass spectrometry, Rapid Commun. Mass Spectrom. 30 (6) (2016) 763–772, https://doi.org/10.1002/rcm.7491.
[15] D. Zuba, Identification of cathinones and other active components of ‘legal highs’ by mass spectrometric methods, Trends Anal. Chem. 32 (2012) 15–30, https://doi.org/10.1016/j.trac.2011.09.009.
[16] E. Fornal, Identification of substituted cathinones: 3,4-Methylenedioxy derivatives by high performance liquid chromatography-quadrupole time of flight mass spectrometry, J. Pharm. Biomed. Anal. 81–82 (2013) 13–19, https://doi.org/10.1016/j.jpba.2013.03.016.
[17] P. Jankovics, A. Varadi, L. Tolgyesi, S. Lohner, J. Nemeth-Palotas, H. Koszegi-Szalai, Identification and characterization of the new designer drug 4'-methylethcathinone (4-MEC) and elaboration of a novel liquid chromatography-tandem mass spectrometry (LC-MS/MS) screening method for seven different methcathinone analogs, Forensic Sci. Int. 210 (2011) 213–220, https://doi.org/10.1016/j.forsciint.2011.03.019.
[18] S. Matsuta, N. Shima, H. Kamata, H. Kakehashi, S. Nakano, K. Sasaki, T. Kamata, H. Nishioka, A. Miki, M. Katagi, K. Zaitsu, T. Sato, H. Tsuchihashi, K. Suzuki, Metabolism of the designer drug alpha-pyrrolidinobutiophenone (alpha-PBP) in humans: identification and quantification of the phase I metabolites in urine, Forensic Sci. Int. 249 (2015) 181–188, https://doi.org/10.1016/j.forsciint.2015.02.004.
[19] C. Sauer, F.T. Peters, C. Haas, M.R. Meyer, G. Fritschi, H.H. Maurer, New designer drug alpha-pyrrolidinovalerophenone (PVP): studies on its metabolism and toxicological detection in rat urine using gas chromatographic/mass spectrometric techniques, J. Mass Spectrom. 44 (6) (2009) 952–964, https://doi.org/10.1002/jms.1571.
[20] Y. Abiedalla, J. DeRuiter, C.R. Clark, GC–MS, GC–MS/MS and GC-IR differentiation of carbonyl modified analogues of MDPV, Forens. Chem. 3 (2017) 58–68, https://doi.org/10.1016/j.forc.2016.11.002.
[21] K. Hasegawa, O. Suzuki, A. Wurita, K. Minakata, I. Yamagishi, H. Nozawa, K. Gonmori, K. Watanabe, Postmortem distribution of α-pyrrolidinovalerophenone and its metabolite in body fluids and solid tissues in a fatal poisoning case measured by LC–MS–MS with the standard addition method, Forensic Toxicol. 32 (2) (2014) 225–234, https://doi.org/10.1007/s11419-014-0227-8.
[22] B. Waters, N. Ikematsu, K. Hara, H. Fujii, T. Tokuyasu, M. Takayama, A. Matsusue, M. Kashiwagi, S. Kubo, GC-PCI-MS/MS and LC-ESI-MS/MS databases for the detection of 104 psychotropic compounds (synthetic cannabinoids, synthetic cathinones, phenethylamine derivatives), Leg. Med. 20 (2016) 1–7, https://doi.org/10.1016/j.legalmed.2016.02.006.
[23] M. Concheiro, S. Anizan, K. Ellefsen, M.A. Huestis, Simultaneous quantification of 28 synthetic cathinones and metabolites in urine by liquid chromatography-high resolution mass spectrometry, Anal. Bioanal. Chem. 405 (29) (2013) 9437–9448, https://doi.org/10.1007/s00216-013-7386-z.
[24] M. Paillet-Loilier, A. Cesbron, R. Le Boisselier, J. Bourgine, D. Debruyne, Emerging drugs of abuse: current perspectives on substituted cathinones, Subst. Abuse Rehabil. 5 (2014) 37–52, https://doi.org/10.2147/SAR.S37257.
[25] D. Ammann, J.M. McLaren, D. Gerostamoulos, J. Beyer, Detection and quantification of new designer drugs in human blood: Part 2 - Designer cathinones, J. Anal. Toxicol. 36 (6) (2012) 381–389, https://doi.org/10.1093/jat/bks049.
[26] M.J. Swortwood, K.N. Ellefsen, A. Wohlfarth, X. Diao, M. Concheiro-Guisan, R. Kronstrand, M.A. Huestis, First metabolic profile of PV8, a novel synthetic cathinone, in human hepatocytes and urine by high-resolution mass spectrometry, Anal. Bioanal. Chem. 408 (18) (2016) 4845–4856, https://doi.org/10.1007/s00216-016-9599-4.
[27] M. Ibanez, O.J. Pozo, J.V. Sancho, T. Orengo, G. Haro, F. Hernandez, Analytical strategy to investigate 3,4-methylenedioxypyrovalerone (MDPV) metabolites in consumers' urine by high-resolution mass spectrometry, Anal. Bioanal. Chem. 408 (1) (2016) 151–164, https://doi.org/10.1007/s00216-015-9088-1.
[28] O.J. Pozo, M. Ibanez, J.V. Sancho, J. Lahoz-Beneytez, M. Farre, E. Papaseit, R. de la

Torre, F. Hernandez, Mass spectrometric evaluation of mephedrone in vivo human metabolism: identification of phase I and phase II metabolites, including a novel succinyl conjugate, Drug Metab. Dispos. 43 (2) (2015) 248–257, https://doi.org/10.1124/dmd.114.061416.

[29] D. Fabregat-Safont, X. Carbón, C. Gil, M. Ventura, J.V. Sancho, F. Hernández, M. Ibáñez, Reporting the novel synthetic cathinone 5-PPDI through its analytical characterization by mass spectrometry and nuclear magnetic resonance, Forensic Toxicol. 36 (2) (2018) 447–457, https://doi.org/10.1007/s11419-018-0422-0.

[30] Z. Qian, W. Jia, T. Li, Z. Hua, C. Liu, Identification of five pyrrolidinyl substituted cathinones and the collision-induced dissociation of electrospray-generated pyrrolidinyl substituted cathinones, Drug Test. Anal. 9 (5) (2017) 778–787, https://doi.org/10.1002/dta.2035.

[31] L. Bijlsma, J.V. Sancho, F. Hernandez, W.M. Niessen, Fragmentation pathways of drugs of abuse and their metabolites based on QTOF MS/MS and MS^E Eaccurate-mass spectra, J. Mass Spectrom. 46 (9) (2011) 865–875, https://doi.org/10.1002/jms.1963.

[32] J.D. Power, S.D. McDermott, B. Talbot, J.E. O'Brien, P. Kavanagh, The analysis of amphetamine-like cathinone derivatives using positive electrospray ionization with in-source collision-induced dissociation, Rapid Commun. Mass Spectrom. 26 (22) (2012) 2601–2611, https://doi.org/10.1002/rcm.6383.

[33] J. Martens, G. Berden, C.R. Gebhardt, J. Oomens, Infrared ion spectroscopy in a modified quadrupole ion trap mass spectrometer at the FELIX free electron laser laboratory, Rev. Sci. Instrum. 87 (10) (2016) 103108, , https://doi.org/10.1063/1.4964703.

[34] M.J. Frisch, G.W. Trucks, H.B. Schlegel, et al., Gaussian 09, Revision A.02.Wallingford, Gaussian, Inc CT, 2016.

[35] L. Sleno, D. Volmer, Ion activation methods for tandem mass spectrometry, J. Mass Spectrom. 39 (2004) 1091–1112.

[36] E. Fornal, Formation of odd-electron product ions in collision-induced fragmentation of electrospray-generated protonated cathinone derivatives: aryl alpha-primary amino ketones, Rapid Commun. Mass Spectrom. 27 (16) (2013) 1858–1866, https://doi.org/10.1002/rcm.6635.

[37] E. Fornal, Study of collision-induced dissociation of electrospray-generated protonated cathinones, Drug Test. Anal. 6 (2014) 705–715, https://doi.org/10.1002/dta.1573.

[38] P.N. Rylander, S. Meyerson, H.M. Grubb, Organic Ions in the Gas Phase. II. The Tropylium Ion, J. Am. Chem. Soc. 79 (4) (1956) 842–846.

[39] F.W. McLafferty, J. Winkler, Gaseous Tropylium, Benzyl, Tolyl, and Norbornadienyl Cations, J. Am. Chem. Soc. 96 (16) (1974) 5182–5189.

[40] F.W. McLafferty, F.M. Bockhoff, Formation of Benzyl and Tropylium Ions from Gaseous Toluene and Cycloheptatriene Cations, J. Am. Chem. Soc. 101 (7) (1979) 1783–1786.

[41] C. Lifshitz, Tropylium Ion Formation from Toluene: Solution of an Old Problem in Organic Mass Spectrometry, Acc. Chem. Res. 27 (1994) 138–144.

[42] M.J. Hayward, F.D.S. Park, L.M. Phelan, S.L. Bernasek, Ä. Somogyi, V.H. Wysocki, Examination of Sputtered Ion Mechanisms Leading to the Formation of C_7H_7, J. Am. Chem. Soc. 118 (35) (1996) 8375–8380.

[43] M.C. Cone, J.S. Dewar, D. Landman, Gaseous Ions. 1. MINDO/3 Study of the Rearrangement of Benzyl Cation to Tropylium, J. Am. Chem. Soc. 99 (1977) (2).

[44] M.J.S. Dewar, D. Landman, Gaseous Ions. 2.1 MINDO/3 Study of the Rearrangements of Toluene and Cycloheptatriene Molecular Ions and the Formation of Tropylium, J. Am. Chem. Soc. 99 (1977) (8).

[45] B.J. Smith, N.E. Hall, G2(MP2, SVP) study of the relationship between the benzyl and tropyl radicals, and their cation analogues, Chem. Phys. Lett. 279 (1997) 165–171.

[46] I.S. Ignatyev, T. Sundius, Competitive ring hydride shifts and tolyl-benzyl rearrangements in tolyl and silatolyl cations, Chem. Phys. Lett. 326 (2000) 101–108.

[47] K.W. Bullins, T.T.S. Huang, S.J. Kirkby, Theoretical investigation of the formation of the tropylium ion from the toluene radical cation, Int. J. Quantum Chem. 109 (6) (2009) 1322–1327, https://doi.org/10.1002/qua.21956.

[48] T.D. Fridgen, J. Troe, A.A. Viggiano, A.J. Midey, S. Williams, T.B. McMahon, Experimental and Theoretical Studies of the Benzylium+/Tropylium+ Ratios after Charge Transfer to Ethylbenzene, J. Phys. Chem. A. 108 (2004) 5600–5609.

[49] M. Vala, J. Oomens, G. Berden, Structure and Dissociation Pathways of Protonated Tetralin (1,2,3,4-Tetrahydronaphthalene), J. Phys. Chem. A. 121 (24) (2017) 4606–4612, https://doi.org/10.1021/acs.jpca.7b01858.

[50] A. Wurita, K. Hasegawa, K. Minakata, K. Gonmori, H. Nozawa, I. Yamagishi, O. Suzuki, K. Watanabe, Postmortem distribution of alpha-pyrrolidinobutiophenone in body fluids and solid tissues of a human cadaver, Leg. Med. 16 (5) (2014) 241–246, https://doi.org/10.1016/j.legalmed.2014.05.001.

[51] S.A. McLuckey, D.E. Goeringer, Slow Heating Methods in Tandem Mass Spectrometry, Int. J. Mass Spectrom. 32 (1997) 461–474.

[52] J. Mitchell Wells, S.A. McLuckey, Collision-Induced Dissociation (CID) of Peptides and Proteins, Method. Enzymol. (2005) 148–185.